# Redox conditions across the Cambrian–Ordovician boundary: elemental and isotopic signatures retained in the GSSP carbonates

Karem Azmy [a*], Brian Kendall [b], Uwe Brand [c], Svend Stouge [d], Gwyneth W. Gordon [e]

[a] Department of Earth Sciences, Memorial University of Newfoundland, St. John's, NL, Canada A1B 3X5, e-mail: kazmy@mun.ca.

[b] Department of Earth and Environmental Sciences, University of Waterloo, Waterloo, ON, Canada N2L 3G1.

[c] Department of Earth Sciences, Brock University, St. Catharines, ON, Canada L2S 3A1

[d] Geological Museum, University of Copenhagen, Øster Voldgade 5, DK-1350 Copenhagen K, Denmark.

[e] School of Earth and Space Exploration, Arizona State University, Tempe, AZ, USA, 85287

Manuscript Accepted for *Palaeogeography, Palaeoclimatology, Palaeoecology*

2015

http://dx.doi.org/10.1016/j.palaeo.2015.09.014

## Abstract

Lime mudstone samples (rhythmites) were collected at high resolution from outcrops of the Cambrian–Ordovician GSSP boundary section at Green Point (western Newfoundland, Canada). The sequence (~ 45 m-thick) consists of slope carbonates with alternating shale and siltstone interbeds, and it spans the boundary located between the Martin Point and Broom Point members

of the Green Point Formation (Cow Head Group). Samples were extracted from micritic rhythmites by microdrilling and subsequently screened using petrographic and geochemical criteria to evaluate their degree of preservation. Although the $\delta^{13}C_{org}$ profile (-29.7 to -25.6 ‰ VPDB) shows insignificant variations, the TOC values (0.1 to 4.1 %) exhibit a generally upward decreasing trend. A negative $\delta^{13}C_{carb}$ excursion, reflecting a sealevel rise, marks a geochemical anomaly that correlates with an increase in the N contents (0 to 2.9 %) of organic matter and the $\delta^{15}N_{org}$ values (-0.6 to +6.0 ‰), which suggests a change to more reducing oceanic conditions. The U contents vary from 0.1 to 3.0 ppm and the $\delta^{238}U$ values (-0.97 to -0.18 ‰) generally decrease with the negative $\delta^{13}C_{carb}$ excursion. The U isotopic variations suggest a widespread increase in reducing conditions associated with sealevel rise during this interval. The investigated sedimentary rocks were slope carbonates where local dysoxic conditions dominated throughout the entire section. Therefore, the changes in the TOC, N, $\delta^{15}N_{org}$, and $\delta^{238}U$ profiles across the boundary are not as sharp as would be expected by a local change from oxic shallow-water to dysoxic/anoxic deep-water settings.

**Key words**: Cambrian–Ordovician GSSP, REE, redox conditions, organic C- and N-isotopes, U-isotopes, western Newfoundland (Canada).

## 1. Introduction

Chemostratigraphy has great potential to refine global stratigraphic correlations of sedimentary sequences. Preserved primary/near-primary stable isotope signatures in marine carbonates, which are associated with time events, provide high-resolution profiles for correlating sedimentary sequences from different depositional settings and paleocontinents (e.g., Veizer et al., 1999;

Halverson et al., 2005; Immenhauser et al., 2008, Azmy et al., 2010). Earlier studies indicated that global sealevel changes along the eastern Laurentian margin around the Cambrian–Ordovician boundary influenced seawater redox conditions and organic productivity (e.g., Landing, 2012; Landing, 2013; Terfelt et al., 2012, 2014; Azmy et al., 2014). Those eustatic sealevel changes influenced the preservation of organic matter by reducing oceanic circulation and intensifying and thickening the mid-water dysoxic layer. The Cambrian–Ordovician boundary interval at Green Point may represent the late part of the so-called long-term "Hatch Hill dysoxic/anoxic interval" that began in the latest early Cambrian (Landing et al., 2002; Landing, 2012, 2013).

Sealevel changes also influence riverine inputs into the oceans and consequently the contents of trace elements in marine deposits (e.g., Wignall and Twitchett, 1996; Murphy et al., 2000; Arnaboldi and Meyers, 2007; Wignall et al., 2007; Piper and Calvert, 2009). The drop of oxygen level in seawater and the spread of dysoxic/anoxic conditions are known to be associated with global reduction of primary productivity and consequently the total organic carbon contents (TOC) and C- and N-isotope compositions of organic matter (e.g., Quan et al., 2008; Herrmann et al., 2012; Quan et al., 2013). Changes in global ocean redox conditions can be inferred from the $\delta^{238}U$ values of marine carbonates and organic-rich mudrocks (e.g., Weyer et al., 2008; Montoya-Pino et al., 2010; Brennecka et al., 2011; Asael et al., 2013; Kendall et al., 2013; Romaniello et al., 2013; Andersen et al., 2014; Dahl et al., 2014; Kendall et al., 2015). The Cambrian–Ordovician GSSP boundary section of Green Point (western Newfoundland, Canada) consists of slope deposits (rhythmites) of deep settings (James and Stevens, 1986) where dysoxic conditions are expected to be dominant (James and Stevens, 1986; Landing et al., 2002; Landing, 2012, 2013). The main objective of the current study is to investigate the C- and N-isotope

compositions of the organic matter in the lime mudstone rhythmites and the associated U-isotope compositions of those marine carbonates to understand changes in global ocean paleoredox conditions that occurred around that time interval.

## 2. Geologic setting

The Paleozoic sedimentary rocks of western Newfoundland in Canada (Fig. 1) were deposited on the eastern Laurentian margin (James et al., 1989). The Laurentian paleoplate developed by active rifting around 570 to 512 Ma (Cawood et al., 2001; Hibbard, 2007; Landing, 2007), and a pre–platform shelf formed and was covered by clastics (James et al., 1989). A major transgression flooded the Laurentian platform margin, which resulted in the accumulation of thick carbonate platform deposits (Wilson et al., 1992; Lavoie et al., 2013). Platform deposits were dominated by high-energy carbonates during the Middle and Late Cambrian (Port au Port Group, western Newfoundland, and evolved into low-energy carbonates of the St. George Group (western Newfoundland) during the Early to earliest Middle Ordovician (cf. Knight et al., 2007, 2008; Lavoie et al., 2013).

## 3. Litho- and Biostratigraphy

Lithostratigraphy of the GSSP Cambrian–Ordovician boundary section in Green Point (western Newfoundland), which is a part of the Green Point Formation of the Cow Head Group (Fig. 2), has been studied and discussed in detail by James and Stevens (1986) and it will therefore be only summarized here. It consists of the uppermost Cambrian (Martin Point Member) and lowermost Ordovician (Broom Point Member), which are generally composed of dark grey to black fissile shale alternating with thin (~ 1 cm-thick) interbeds of ribbon limestone rhythmites. Siltstone interbeds (up to 1 cm thick) may co-occur with shales, and the limestone

interbeds vary from isolated to combined layers of up to 20 cm. The conglomerate beds contain blocks of shallow water carbonates that were transported into the deep-water facies along the slope of the Laurentian margin (James and Stevens, 1986).

The Cambrian–Ordovician GSSP section at Green Point spans the *Cordylodus proavus* (Furongian, uppermost Cambrian) to the *Cordylodus angulatus* Zones (Tremadocian, Lower Ordovician). The Cambrian–Ordovician boundary is defined by the First Appearance Datum (FAD) of the conodont *Iapetognathus fluctivagus* (Barnes, 1988; Cooper et al., 2001). The current spike marking the Cambrian–Ordovician boundary in the GSSP section at Green Point is placed within Bed 23 slightly above the base of the negative $\delta^{13}C_{carb}$ excursion that marks a geochemical anomaly (Fig. 2; Azmy et al., 2014).

## 4. Methodology

Samples (Appendix 1, Fig. 2) were collected at high resolution (sampling intervals as small as 10 cm) from the Cambrian–Ordovician GSSP boundary section (49° 40′ 51″ N; 57° 57′ 36″ W) at Green Point, western Newfoundland (Fig. 1). They were taken from the laminated lime mudstone rhythmites to avoid allochthonous clasts (Fig. 3a,b). Thin sections of samples were examined petrographically with a polarizing microscope (cf. Azmy et al., 2014) and stained with Alizarin Red–S and potassium ferricyanide solutions (Dickson, 1966). Cathodoluminescence (CL) observations were performed using a Technosyn 8200 MKII cold cathode instrument operated at 8 kV accelerating voltage and 0.7 mA current.

A mirror-image slab of each thin section was also prepared and polished for microsampling. Polished slabs were washed with deionized water and dried overnight at 50 $^{o}$C prior to isolating

the finest grained micritic lime mudstone free of secondary cements. Up to 10 g of powder were extracted from the finest grain material.

For elemental analyses, a subset of sample powder was digested in 5 % (v/v) acetic acid for 70–80 min. and analysed for major, minor and rare earth elements (REE) using an Elan DRC II ICP-MS (Perkin Elmer SCIEX) at Memorial University of Newfoundland. International (DLS-88a and CCH-1) and internal standards were utilized to normalize the results. The relative uncertainties of these measurements are better than 5%, and results are normalized to a 100 % carbonate basis.

Organic carbon- and nitrogen-isotope ratios were measured on isolated kerogen after repeated treatment with pure concentrated hydrochloric acid at the isotope laboratory of Memorial University of Newfoundland, using a Carlo Erba Elemental Analyzer coupled to a ThermoFinnigan DELTA V plus isotope ratio mass spectrometer in a stream of helium, where the gas was ionized and measured for isotope ratios. The results were normalized to the standards IAEA-CH-6 ($\delta^{13}C$ = -10.43‰ VPDB), NBS18 ($\delta^{13}C$ = -5.04‰ VPDB), USGS24 ($\delta^{13}C$ = -15.99‰ VPDB), IAEA-N-1 ($\delta^{15}N$= 0.43‰ air), and IAEA-N-2 ($\delta^{15}N$= 20.32‰ air). The uncertainty calculated from repeated measurements was ~ 0.2 ‰.

Uranium isotope measurements were carried out at the W.M. Keck Foundation Laboratory for Environmental Biogeochemistry, School of Earth and Space Exploration, Arizona State University. Between 2 and 9 g of powdered sample was first ashed at 750°C to calcinate the carbonate matrix, thus destroying all organic matter (Romaniello et al., 2013). A cold leach with dilute 1M HCl and then 1M $HNO_3$ was used to extract authigenic U from the samples while minimizing inclusion of detrital material. A portion of the sample solution corresponding to

approximately 500 ng of U was equilibrated with a double spike ($^{233}U$-$^{236}U$; IRMM3636; Verbruggen et al., 2008; Romaniello et al., 2013) by reacting the sample-spike mixture in concentrated $HNO_3$ and HCl. The sample-spike mixture was passed through UTEVA resin to separate U (Weyer et al., 2008). After column chemistry, samples were reacted with a $HNO_3$-$H_2O_2$ mixture to destroy residual organic material from the UTEVA resin (Romaniello et al., 2013). Samples were re-dissolved in 2% $HNO_3$ and analyzed on a multi-collector inductively coupled plasma mass spectrometer (MC-ICP-MS; Thermo Scientific Neptune) using an ESI Apex desolvating nebulizer (Kendall et al., 2013; Romaniello et al., 2013). The U concentration of each sample was calculated using double spike isotope dilution analysis. Sample $\delta^{238}U$ was reported relative to the CRM 145 standard as follows (Romaniello et al., 2013):

$$\delta^{238}U\ (‰) = [(^{238/235}U_{sample} / {}^{238/235}U_{CRM\ 145}) - 1] \times 1000$$

Instrument accuracy and precision was verified by analysis of the secondary standards SRM 950a and CRM 129a. During the course of this study, the average $\delta^{238}U$ for SRM 950a and CRM 129a was 0.01±0.11 ‰ (2SD, n=4) and -1.71±0.08 ‰ (2SD, n=16), respectively. This is in excellent agreement with previous studies that determined the values of SRM 950a and CRM 145 to be statistically indistinguishable (Weyer et al., 2008; Condon et al., 2010; Kendall et al., 2013), and with previous measurements of CRM 129a (Brennecka et al., 2011; Kendall et al., 2013). Based on the reproducibility of the more frequently measured CRM 129a standard, the 2σ uncertainty of a sample measured in the current study is the 2σ uncertainty of sample replicate measurements or 0.08 ‰, whichever is greater. Other recent studies using the Thermo Scientific Neptune at Arizona State University report similar uncertainties for CRM 129a (Kendall et al., 2013, 2015). Most samples were run at least in duplicate during different mass spectrometry

sessions, with the exception of a few samples for which inadequate solution was available. In addition, $\delta^{234}U$ was measured simultaneously with $\delta^{238}U$ using the procedure of Romaniello et al. (2013), and is reported as:

$$\delta^{234}U\ (‰) = [(^{234/238}U_{sample} / {}^{234/238}U_{CRM\ 145}) - 1] \times 1000$$

Relative to secular equilibrium, CRM 145 has a value of -36‰ to -37‰ (Andersen et al., 2004). The value of CRM 145 was set to -36.7 ‰ (Romaniello et al., 2013). As the samples analyzed in this study are from the Cambrian–Ordovician GSSP, the U isotope systematics should be in secular equilibrium provided that samples have not been recently disturbed during the past ~2 Ma, and thus should have $\delta^{234}U$ values close to 0‰. Full powder replicates for three samples (GP 2, GP 28, and GP 59) demonstrate excellent reproducibility for both $\delta^{238}U$ and $\delta^{234}U$.

## 5. Results

Petrographic examinations indicated that the examined material was dominantly micritic carbonate rhythmites with < 1% disseminated microrhombic pyrite of most likely microbial origin and an earlier study (Azmy et al., 2014) indicated that there is a negative $\delta^{13}C_{carb}$ excursion, which starts at a stratigraphic level slightly below the suggested biostratigraphic boundary (Figs. 2 and 4). Table 1 summarizes the statistics of geochemical results of the GSSP Cambrian–Ordovician boundary carbonate rhythmites. The total organic content (TOC) varies between 0.1 and 4.1 % and the $\delta^{13}C_{org}$ signatures vary from -25.6 to -29.7 ‰ (VPDB). Mean values of $\delta^{13}C_{org}$ in the beds below the $\delta^{13}C_{carb}$ excursion and those correlated with the excursion (cf. Azmy et al., 2014) are almost the same (-27.2±1.2 ‰ and -27.8±1.1 ‰ VPDB, respectively; Table 1). By contrast, the mean TOC contents are lower in the beds correlated with the $\delta^{13}C_{carb}$ excursion (0.6±0.5 vs. 1.7±0.9 wt. %, Table 1). The TOC contents are generally within the range

documented for shales from around the Cambrian–Ordovician boundary in many locations in western Newfoundland (0.6 to 5.2 wt. %; Weaver et al., 1988). Similarly, their $\delta^{13}C_{org}$ values are consistent with those documented for crude oil seeps from the same shales (-28.2 to -33.0 ‰; Weaver et al., 1988).

The $\delta^{15}N_{org}$ signatures range from -0.6 to +6.0 ‰ (Table 1) where the most depleted values are lower than those documented for present-day Black Sea sediments (~3 ‰, Fry et al., 1991; Çoban-Yıldız et al., 2006) and modern marine biomass and nitrates (~5 ‰, Galbraith et al., 2008). The GSSP $\delta^{15}N_{org}$ values are also within the range documented for kerogen extracted from shales of the same age in western Newfoundland (-1.2 to -7.1 ‰; Weaver et al., 1988). The mean $\delta^{15}N$ values (1.2±1.2 ‰) of the carbonate beds below the geochemical anomaly, marked by the start of the negative $\delta^{13}C_{carb}$ excursion (Azmy et al., 2014), are generally lower than that of their counterparts above the anomaly (2.8±1.5 ‰, Table 1 and Fig. 4).

The U concentrations vary between 0.1 and 4.3 ppm (Table 1). The $\delta^{238}U$ values vary between -0.18 and -0.97 ‰ and there is a noticeable decrease from -0.28±0.11 ‰ below the geochemical anomaly level to -0.58±0.18 ‰ during the negative $\delta^{13}C_{carb}$ excursion (Fig. 4 and Table 1). With respect to $\delta^{234}U$, most samples fall within 15‰ of secular equilibrium. There is no correlation between $\delta^{234}U$ and $\delta^{238}U$ or between U concentrations and $\delta^{234}U$ ($R^2 < 0.1$). A moderate correlation occurs between U concentrations and $\delta^{238}U$ ($R^2 = 0.47$).

## 6. Discussion

### *6.1. Evaluation of sample preservation*

#### 6.1.1. Petrographic preservation

195 Petrography and preservation of micritic fabric of the investigated samples have been
196 discussed in detail by Azmy et al. (2014) and are summarized below. Except for two samples
197 around the top of Bed 18 in the middle of the Martin Point Member that contained laminae of
198 argillaceous carbonates (Samples GP11 and GP12, Appendix 1), the Green Point Formation at
199 the Cambrian–Ordovician GSSP is dominated by fabric retentive lime mudstones (rhythmites of
200 micritic to near-micritic grain size) with insignificant recrystallization (Fig. 3a) and no- to dull
201 luminescence under cold cathodoluminoscope (Fig. 3b). These observations suggest a high
202 degree of petrographic preservation (Azmy et al., 2014). Luminescence in carbonates is mainly
203 activated by high concentrations of Mn and quenched by high concentrations of Fe (Machel and
204 Burton, 1991). Although dull luminescence may indicate relatively good preservation of
205 geochemical signatures, altered carbonates may still exhibit no luminescence due to high-Fe
206 content (Rush and Chafetz, 1990). Therefore, cathodoluminescence is a single evaluation tool
207 that has to be confirmed by other screening tests (Brand et al., 2011).

208 6.1.2. Geochemical Preservation

209 Preservation of the elemental geochemical signatures in the investigated samples has been
210 discussed in detail by Azmy et al. (2014). The progressive burial of sediments during the
211 diagenetic history of basins is associated with an increase in temperature (>50 ºC), which leads
212 to a thermal degradation of the organic matter and a decrease in the TOC that becomes
213 isotopically heavier as $^{12}C$-enriched organic compounds are released (e.g., Popp et al., 1997;
214 Faure and Mensing, 2005). The insignificant correlations ($R^2$=0.01) between the $\delta^{13}C_{org}$ and
215 TOC wt. % values (Fig. 5a) argues against significant bio- and thermal degradation and is
216 consistent with preservation of the micritic texture, thus suggesting a high degree of preservation
217 of the $\delta^{13}C_{org}$ signatures. This is consistent with the poor correlation between the $\delta^{15}N_{org}$ and

TOC wt. % values (Fig. 5b; e.g., Yamaguchi et al., 2010), which also supports the preservation of the $\delta^{15}N_{org}$ signatures. Limited deviation in $\delta^{234}U$ from secular equilibrium, together with the absence of a correlation between $\delta^{234}U$ and $\delta^{238}U$, points to minimal modification of $\delta^{238}U$ signatures by recent fluid flow during the past ~2 Ma. Also, the insignificant correlations ($R^2 < 0.1$) between elements known to be enriched in crustal clastic rocks, such as Al and Ti, with the $\delta^{238}U$ values (Appendix 1) argues for the primarily authigenic nature of those isotope signatures in the carbonates and minimal overprint by silicate inclusions.

### *6.2. Elemental variations*

Variations in sealevel, particularly those related to time events, are generally associated with changes in trace and rare earth element (REE) concentrations in sediments due to inputs of terrestrial material and/or changes in redox conditions (e.g., Wignall and Twitchett, 1996; Murphy et al., 2000; Kimura et al., 2005; Arnaboldi and Meyers, 2007; Wignall et al., 2007; Piper and Calvert, 2009; Śliwiński et al., 2010; Dickson et al., 2012). Therefore, major $\delta^{13}C_{carb}$ shifts of remarkable time events reflect relative changes in organic productivity and paleoredox conditions (e.g., Azmy et al., 2014). An earlier detailed study of the $\delta^{13}C_{carb}$ profile of the GSSP Cambrian–Ordovician boundary at Green Point by Azmy et al. (2014) documented a significant negative excursion (~ 6 ‰) near the top of Bed 22 (Fig. 4). Phosphorous, Cu, and Ni have been utilized as proxies for bioproductivity and V, Cr, Co, Mo, and Th/U for paleoredox (e.g., Hatch and Leventhal, 1992; Wignall and Twitchett, 1996; Falkowski 2004; Morel et al., 2004; Azmy et al., 2012). However, the investigated boundary section at Green Point consists of carbonates deemed to be deposited in slope settings (James and Stevens, 1986) where the abundance of biota below the photic zone is generally low, particularly during the Early Paleozoic, compared

240 with their shallow water counterparts. Also, many of those proxies were formulated based on
241 applications to shales and sapropels that have different mineralogical and chemical compositions
242 from those of carbonates (e.g., Hatch and Leventhal, 1992; Arnaboldi and Meyers, 2007; Zhou et
243 al., 2012). Therefore, the application of elemental proxies to slope carbonates has to be done
244 with caution since not all proxies are expected to show consistent responses similar to those
245 observed in shallow shelf sedimentary rocks.

246 A few samples in the Green Point section exhibit a significant enrichment in P (up to 7914
247 ppm, Samples GP 27 and 28, Appendix 1), which is also coupled with significant enrichment in
248 ∑REE (267 ppm). No other correlated consistent enrichment in other proxies such as V, Cr, Co,
249 Ni, Cu, or Mo has been detected at the boundary level (Appendix 1) since their concentrations
250 are below detection limits (e.g., Co, Ni, Cu) and most of those of V and Cr are below 5 ppm
251 except for a few values (Appendix 1). Although enrichment in P could be attributed to an
252 increase in primary productivity possibly due to increase in terrestrial input of organic matter
253 and/or nutrient input from upwelling currents (e.g., Azmy et al., 2011), the high-P samples in the
254 investigated section were peloidal algal mud to grainstones that contain phosphatic laminated
255 algae or aggregates, which most likely resulted in the high P contents (Azmy et al., 2014). Those
256 few high P samples have also high total REE (∑REE) contents (Appendix 1) where REE are
257 known to be enriched particularly in biogenic phosphates (e.g., Lécuyer et al, 1998). The scarcity
258 of high P samples is also consistent with the expected low density of terrestrial plants (source of
259 organic matter) during the late Cambrian to early Ordovician (e.g., Davis and Gibling, 2010).

260 High Al and Si values around the top of Bed 18 in the middle of the Martin Point Member
261 are associated with argillaceous carbonates (Samples GP11 and GP12, Appendix 1) and do not

correlate with P or ∑REE contents. These variations may reflect an abrupt input of siliciclastics into the slope carbonates possibly due to short-term turbidity particularly with the lack of correlation with a time event or influence on the $\delta^{13}C$ values (Azmy et al., 2014).

Levels of oxygen in the water column influence the oxidation state of redox-sensitive elements and selectively control their solubility in seawater and consequently their degree of enrichment in marine sediments (e.g., Wignall and Twitchett, 1996; Kimura et al., 2005; Tribovillard et al., 2006; Arnaboldi and Meyers, 2007, Wignall et al., 2007). In oxidizing environments, uranium ions maintain the higher oxidation state ($U^{+6}$) and form uranyl carbonate, which is soluble in water whereas in reducing conditions, they retain the lower oxidation state ($U^{+4}$) and form the insoluble uranous fluoride which is trapped into marine carbonates (Wignall and Twitchett, 1996). In contrast, thorium is not affected by redox conditions in the water column and occurs permanently in the insoluble $Th^{+4}$ state. Accordingly, sediments of anoxic environments are richer in uranium and have lower Th/U than those of oxic environments. Therefore, the Th/U ratio has been used as a proxy for environmental redox conditions, with ratios < 2 in anoxic marine sediments and > 2 in oxic sediments (cf. Wignall and Twitchett, 1996). The Th/U values of the Green Point carbonates are < 2 throughout the entire boundary section, thus reflecting reducing conditions. However, the Y/Ho (proxy of preservation of REE composition of carbonates; Webb and Kamber, 2000) values of the Green Point carbonates (34±5) are lower than those suggested for Holocene marine carbonates (≥ 50, Webb and Kamber, 2000; Azmy et al., 2014), which implies minor alteration of the elemental geochemical signatures even at low water/rock ratios. Therefore, the interpretation of the Th/U values has to be taken with some caution, particularly when ratios of < 2 are associated with occurrences of phosphatic algae that cannot tolerate reducing conditions (Azmy et al., 2014).

285 Cerium anomalies provide complementary information on local redox conditions. The
286 Ce/Ce* values of the Green Point carbonates are higher than the range documented for Holocene
287 microbialites of well-oxygenated shallow water settings, and thus record more reducing
288 conditions (Webb and Kamber, 2000; Fig. 6). However, a small number of values falls within the
289 Holocene Ce/Ce* range of shallow water microbilaites although they have lower Y/Ho ratios.
290 The relatively higher Ce/Ce* values are expected for slope carbonates because Ce is oxidized in
291 shallow oxic water into $CeO_2$, which is scavenged by organic matter leaving shallow water
292 depleted in Ce. Shallow-water carbonates thus have lower Ce/Ce* values than those of relatively
293 deeper water settings (e.g., Alibo and Nozaki, 1999). The generally high Ce/Ce* values
294 (0.86±0.06) of the Green Point carbonates are <1 and they therefore possibly reflect
295 suboxic/dysoxic conditions rather than anoxia (Webb and Kamber, 2000); a condition
296 reconcilable with the low Th/U ratios (<2) and the occurrence of phosphatic algae.

297 The low pyrite content in the GSSP boundary section (< 1%) supports dysoxic rather than
298 anoxic conditions in local bottom waters. This suggests that the drop in the oxygen level led to
299 reduction in primary productivity but was not severe enough to reach extinction levels, which is
300 consistent with the paleontological evidence (cf. Cooper et al., 2001; Terfelt et al., 2014).

301 6.3. *Organic C- and N-isotopes*

302 The $\delta^{13}C_{org}$ profile of the GSSP at Green Point shows wide variations of up to 4 ‰ (between
303 ~ -29.7 and -25.6‰ VPDB; Table 1) before the $\delta^{13}C_{carb}$ excursion (Fig. 4). The width of the
304 variations decreases considerably through the upper part of the excursion although the $\delta^{13}C_{org}$
305 profile generally exhibits a parallel trend to its $\delta^{13}C_{carb}$ counterpart particularly at the excursion
306 interval. However, the TOC contents decrease noticeably with the $\delta^{13}C_{carb}$ excursion (Fig. 4) and

their profile starts to increase again at the level above the $\delta^{13}C_{carb}$ shift. The decline in TOC content during the excursion suggests a drop of marine organic productivity particularly for sediments of slope settings where oxidation of organic matter is unlikely. The lack of significant correlation between the $\delta^{13}C_{org}$ and TOC values strongly support the preservation of their signatures (Fig. 5a) and the correlation of the $\delta^{13}C_{carb}$ excursion with lower TOC contents (Fig. 4), compared with those in the lower section, suggests that a sealevel rise led to relative reduction in organic productivity at the Cambrian–Ordovician boundary (Lehnert et al., 2005).

The investigated carbonates have low C/N ratios of <<10 (Table 1 and Appendix 1), which implies insignificant contribution from terrestrial plants and is consistent with the low diversity of land plants during the earliest Phanerozoic (e.g., Meyer, 1994; Theissen et al., 2003). The mean values of N contents show an increase in the beds above the geochemical anomaly level (Table 1) in association with the negative $\delta^{13}C_{carb}$. The $\delta^{15}N_{org}$ profile of the GSSP section also exhibits relative enrichment in $^{15}N$ (~1.6 ‰ higher) in the beds correlated with the $\delta^{13}C_{carb}$ excursion (Table 1 and Fig. 4), which is consistent with a sealevel rise during the Cambrian–Ordovician boundary and with enhanced fractionation due to denitrification (e.g., Quan et al., 2013). The generally low $\delta^{15}N$ values (2.0±1.6 ‰) through the GSSP are comparable with those documented for modern Black Sea sediments (~ 3 ‰), and thus suggest a period of relative stagnation and low primary productivity dominated by suboxic/dysoxic to anoxic conditions (e.g., Quan et al., 2008). This is consistent with the conclusions from the Th/U (<2) values (Appendix 1) and with the Ce/Ce* ratios (near unity) that vary between 0.8 and 1.0 (Fig. 6, Azmy et al., 2014). Despite the isotopic enrichment during active denitrification, the investigated organic matter has $\delta^{15}N$ values depleted relative to modern phytoplankton (~2 to 7

329 ‰, Faure and Mensing, 2005), thus suggesting an influence by $N_2$-fixing bacteria rather than
330 terrestrial inputs, which is also consistent with the low abundance of terrestrial plants around the
331 time of the early Paleozoic (e.g., Davis and Gibling, 2010).

332 *6.4. U-isotopes*

333 Uranium concentrations have been found to vary from an average of ~1.5 ppm in modern
334 shallow marine biogenic carbonates to an average of ~ 4.1 ppm in bulk sediment counterparts
335 (Romaniello et al., 2013). The average concentration of U in the GSSP lime mudstones (1.0±0.8
336 ppm, Table 1) is generally lower than that of modern marine carbonates but there is no clear
337 evidence or a reason to expect depletion of U concentrations in the GSSP carbonates by
338 diagenesis. The near-micritic grain size of the investigated lime mudstone rhythmites argues
339 against significant diagenetic alteration (Azmy et al., 2014). Further evidence against diagenetic
340 alteration is the poor correlation of $\delta^{238}U$ values and also U concentrations with their Sr
341 counterparts (Figs 7a-b), since Sr is well known to become significantly depleted in altered
342 carbonates with progressive diagenesis (Brand and Veizer, 1980; Veizer, 1983). Similarly, no
343 significant correlations of $\delta^{238}U$ values and U concentrations have been found with other
344 elements such as Al, Si or Ti ($R^2 < 0.1$), which argues against inputs from clastic inclusions and
345 their possible influence on the $\delta^{238}U$ signatures.

346 The alternation between organic-rich shales and thin carbonate interbeds in the GSSP section
347 in Green Point possibly caused the U to be preferentially enriched in the shales leaving the local
348 seawater depleted, thus leading to deposition of U-depleted carbonates. This may explain the
349 lower U contents of the GSSP lime mudstone rhythmites relative to their modern Bahamas
350 counterparts (Romaniello et al., 2013) and also supports their primary nature. The partial

restriction in water circulation and in the basin connection to open ocean water during the interval that spans the geochemical anomaly (Cooper et al., 2001; Azmy et al., 2014), as indicated by disappearance and decrease of diversity of some pelagic organisms (Cooper et al., 2001; Terfelt et al., 2012, 2014; Pouille et al., 2014) immediately above the geochemical anomaly level (Fig. 4; Bed 19 to Bed 24), might have also enhanced the depletion of U in the carbonate rhythmites (i.e., because of slow rates of deep-water renewal in the basin).

On the other hand, the low U contents throughout the investigated section may simply reflect dominantly dysoxic rather than anoxic conditions (Wignall and Twitchett, 1996). Uranium (insoluble $U^{+4}$) is generally enriched in black shales with the increase in reducing conditions (Wignall and Twitchett, 1996; Montoya-Pino et al., 2010), and similarly in sulfidic marine carbonates of carbonate-dominant environments such as the Bahamas (Romaniello et al., 2013). Given the lack of pyrite (<1 %) in the GSSP carbonates, lower amounts of dissolved pore water sulfide may explain the lower U contents of the Green Point carbonates compared to Bahamian carbonates. This observation is relevant to the magnitude of U isotope fractionation between seawater and carbonate sediments. As shown for the Bahamas, strong reducing conditions promoted by high dissolved pore water sulfide concentrations leads to the preferential removal of $^{238}U$ relative to $^{235}U$, resulting in bulk carbonate sediments with $\delta^{238}U$ that is 0.2–0.4 ‰ higher than seawater (Romaniello et al., 2013). In the case of the Green Point carbonate rhythmites, the lower levels of dissolved sulfide implied by the low U concentrations and pyrite contents suggests that there was a generally smaller isotopic offset between these carbonates and coeval Cambrian–Ordovician seawater compared to that between the Bahamas and modern seawater.

Although a moderate positive correlation is observed between U concentrations and $\delta^{238}U$ in the carbonates ($R^2 = 0.47$, Fig. 7c), the samples with low U concentrations have $\delta^{238}U$ that falls

well below the range of detrital compositions ($\delta^{238}U$ = -0.51 to -0.20 ‰; Weyer et al., 2008; Telus et al., 2012). Therefore, input of detrital material is unlikely to be the reason for the variations observed in $\delta^{238}U$, which is consistent with petrographic evidence (lack of siliciclastic inclusions), low Al and Si contents, and lack of covariation between $\delta^{238}U$ and Al, Si, and Ti contents (Appendix 1).

The $\delta^{238}U$ values show an overall decrease upsection to ≤ -0.4‰, which is correlated with the negative $\delta^{13}C_{carb}$ excursion and with the increase in $\delta^{15}N_{org}$ values (Fig. 4). The mean $\delta^{238}U$ value (-0.58±0.18 ‰, Table 1) of the carbonate interbeds above the geochemical anomaly level, which marks the base of the $\delta^{13}C_{carb}$ excursion (Fig. 4), is lower than its counterpart below the anomaly level (-0.28±0.11 ‰, Table 1) and thus reflects relative depletion in $^{238}U$ due to sealevel rise (Figs. 2 and 4) and increase in reducing conditions. This change in ocean redox conditions may be widespread because U has a long seawater residence time (~400−500 kyr today; Ku et al., 1977; Dunk et al., 2002) and carbonate $\delta^{238}U$ can reflect global ocean paleoredox conditions (e.g., Brennecka et al., 2011). Below the anomaly, the mean $\delta^{238}U$ value is close to that of modern seawater (-0.40±0.03 ‰; Weyer et al., 2008; Andersen et al., 2014), taking into account the possibility that the Green Point carbonates are offset to slightly heavier U isotope compositions compared to seawater (Romaniello et al., 2013). Hence, the marine U isotope mass balance and extent of ocean oxygenation before the start of the $\delta^{13}C_{carb}$ excursion may have been similar to the modern ocean.

The insignificant correlation between Al and Th/U ($R^2$=0.14) supports the lack of influence of siliciclastic inputs. Although Th/U ratios are below 2 and reflect dysoxic/reducing conditions throughout the entire investigated boundary section, they show a slight change (~0.2) from a

mean value of 0.5 below the geochemical anomaly (Table 1) to 0.7 above the anomaly (Table 1). The drop in the $\delta^{238}U$ values above the anomaly level is correlated with the slight increase in the mean Th/U ratio (Fig. 4 and Table 1). A comparable drop in $\delta^{238}U$ values with a similar rise in the Th/U ratios (~ 0.2), and also associated with a negative $\delta^{13}C_{carb}$ excursion, has been documented in the Upper Permian GSSP (Brennecka et al., 2011). The low $\delta^{238}U$ in the Upper Permian carbonates is believed to reflect a global expansion in anoxic conditions that caused an increase in the preferential removal of heavy $^{238}U$ to organic-rich shales, thus driving seawater $\delta^{238}U$ to lighter values (Brennecka et al., 2011). Consistent with the shift to lower $\delta^{238}U$ values, the increase in Th/U ratios suggests a mild decrease in the global seawater U inventory because of a global expansion in the extent of reducing conditions. However, the overall change in the Th/U ratios across the negative $\delta^{13}C_{carb}$ excursion is small (~0.2) relative to the total variation of Th/U ratios in the Cambrian–Ordovician GSSP boundary section, which suggests that its interpretation has to be taken with caution.

In addition to changes in global ocean paleoredox conditions, deposition of the organic-rich shales in the local marine basin may have affected the isotopic composition of U in the alternating thin carbonate beds. A relative increase in the extent of reducing conditions in the marine basin associated with the negative $\delta^{13}C_{carb}$ excursion may have caused an increase in the extent of preferential removal of the heavier $^{238}U$ isotope from seawater to the organic-rich shales (cf. Weyer et al., 2008; Montoya-Pino et al., 2010; Andersen et al., 2014). Consequently, bottom waters in the basin may have developed lighter $\delta^{238}U$ relative to open ocean seawater, which is reflected in the spatially associated (alternating) carbonate interbeds. The general prevalence of lower $\delta^{238}U$ during the negative $\delta^{13}C_{carb}$ excursion suggests that the implied

418 restriction in the basin connection to the open ocean (Cooper et al., 2001; Azmy et al., 2014)
419 might have contributed to the increase in reducing conditions.

420 This hypothesis is based on observations of the U isotope variations in the euxinic sediments
421 of the modern Black Sea and Cariaco Basin, which are suggested to be related to the extent of U
422 removal from local bottom waters (Weyer et al., 2008; Montoya-Pino et al., 2010; Andersen et
423 al., 2014). Extensive removal of isotopically heavy U to organic-rich sediments during the GSSP
424 Cambrian–Ordovician boundary interval would lead to bottom waters that are isotopically light
425 and depleted in U, which are then captured by the stratigraphically alternating carbonates. By
426 contrast, a smaller extent of isotopically heavy U removal to organic-rich sediments at a time of
427 less reducing conditions will leave bottom waters that are relatively isotopically heavier and
428 more enriched in U. This process can account for the moderate positive correlation between U
429 concentrations and $\delta^{238}U$ in the Green Point carbonates.

430 In summary, despite the well-pronounced change in the $\delta^{13}C_{carb}$ profile across the GSSP
431 boundary section, the changes in the TOC, N, $\delta^{15}N_{org}$ , and $\delta^{238}U$ counterparts are not similarly
432 sharp. The nature of the local sedimentary environment seems to have some control on those
433 proxies since the investigated carbonates were slope deposits where a dysoxic environment
434 dominated. The rise in sealevel was not accompanied by a dramatic change from locally oxic to
435 anoxic conditions but rather a relative increase in the dysoxic conditions, which is supported by
436 the lack of paleontological evidence for a major extinction event.

437

438 **7. Conclusions**

The slope-setting lime mudstone rhythmites of the Cambrian–Ordovician GSSP boundary section in Green Point (western Newfoundland, Canada) exhibit extensive petrographic preservation and retention of, at least, their near-primary geochemical signatures.

The TOC profile across the boundary shows a drop above a geochemical anomaly level that was marked by the start of a documented negative $\delta^{13}C_{carb}$ excursion. Although the $\delta^{13}C_{org}$ profile does not show a distinct change, the $\delta^{15}N_{org}$ profile exhibits an enrichment correlated with the $\delta^{13}C_{carb}$ excursion, which suggests an increase in the reducing/dysoxic conditions due to sealevel rise.

The $\delta^{238}U$ profile shows a decrease in correlation with the $\delta^{13}C_{carb}$ excursion, thus suggesting an enhancement in the reducing conditions, which is consistent with the $\delta^{15}N_{org}$ results. The rhythmic occurrence of organic-rich shale with thin carbonate interbeds may have influenced the $\delta^{238}U$ signatures of the carbonates.

The Ce/Ce* (0.9±0.1) and Th/U (0.6±0.6) ratios, along with N- and U-isotope results, also support the expansion of relatively more dysoxic conditions in correlation with the documented negative $\delta^{13}C_{carb}$ excursion, which is consistent with the occurrence of phosphatic algae in a few beds. This may imply that the change in redox conditions was most likely not severe enough to cause an extinction event, which is in agreement with the lack of paleontological evidences of major faunal extinction and with the invariable low pyrite contents in the carbonate interbeds throughout the GSSP boundary section.

460 **Acknowledgements**

461 The authors wish to thank Drs. Thierry Corrège (editor), Feng Lu (reviewer) and Ed Landing
462 (reviewer) for their constructive reviews. Also, the efforts of Ms. Krishnaveni Kunchala (Journal
463 manager) are much appreciated. This project was supported by funding (to Karem Azmy) from
464 Petroleum Exploration Enhancement Program (PEEP), (to Brian Kendall) from a NSERC
465 Discovery Grant, and (to Svend Stouge) from the Carlsberg Foundation. Stephen Romaniello is
466 thanked for helpful advice regarding U isotope measurements of carbonates, and Ariel Anbar is
467 thanked for generous access to the W.M. Keck Foundation Laboratory for Environmental
468 Biogeochemistry.

469

## References


Alibo, D.S., Nozaki, Y., 1999. Rare earth elements in sweater: particle association, shale-normalization, and Ce Oxidation. Geochim et Cosmochim Acta 63 (3-4), 363–372.

Anbar, A.D., Knab, K.A., Barling, J., 2001. Precise determination of mass-dependent variations in the isotopic composition of molybdenum using MC-ICPMS. Analytical Chemestry 73, 1425–1431.

Andersen, M.B., Romaniello, S., Vance, D., Little, S.H., Herdman, R., Lyons, T.W., 2014. A modern framework for the interpretation of $^{238}U/^{235}U$ in studies of ancient ocean redox. Earth and Planetary Science Letters 400, 184-194.

Arnaboldi, M., Meyers, P.A., 2007. Trace element indicators of increased primary production and decreased water-column ventilation during deposition of latest Pliocene sapropels at five locations across the Mediterranean Sea. Palaeogeography, Palaeoclimatology, Palaeoecology 249, 425–443.

Asael, D., Tissot, F.L.H., Reinhard, C.T., Rouxel, O., Dauphas, N., Lyons, T.W., Ponzevera, E., Liorzou, C., Chéron, S., 2013. Coupled molybdenum, iron and uranium stable isotopes as oceanic paleoredox proxies during the Paleoproterozoic Shunga Event. Chem. Geol. 362, 193-210.

Azmy, K., Brand, U., Sylvester, P., Gleeson, S., Logan, A., Bitner, M.A., 2011. Biogenic low–Mg calcite (brachiopods): proxy of seawater–REE composition, natural processes and diagenetic alteration. Chemical Geology 280, 180−190.

Azmy, K., Mottequin, B., Poty, E., 2012. Frasnian-Famenian pre-event: a record from the Dinant Basin, Belgium. Palaeogeography, Palaeoclimatology, Palaeoecology 313, 93-106.

Azmy, K., Stouge, S., Brand, U., Bagnoli, G., 2014. High-resolution chemostratigraphy of the Cambrian–Ordovician GSSP in western Newfoundland, Canada: enhanced global correlation tool. Palaeogeography, Palaeoclimatology, Palaeoecology 409, 135-144.

Azmy, K., Stouge, S., Christiansen, J.L., Harper, D.A.T., Knight, I., Boyce, D., 2010. Carbon-isotope stratigraphy of the Lower Ordovician succession in Northeast Greenland: implications for correlations with St. George Group in western Newfoundland (Canada) and beyond. Sedimentary Geology 225, 67−81.

Barnes, C.R., 1988. The proposed Cambrian–Ordovician global boundary stratotype and point (GSSP) in western Newfoundland, Canada: Geological Magazine 125, 381-414.

Bau, M., and Dulski, P., 1996, Distribution of yttrium and rare-earth elements in the Penge and Kuruman iron-formations, Transvaal Supergroup, South Africa: Precambrian Research 79, 37–55.

Brand, U., Veizer, J., 1980. Chemical diagenesis of a multicomponent carbonate system: 1. Trace elements. Journal of Sedimentary Petrology 50, 1219–1236.

Brand, U., Logan, A., Bitner, M.A., Griesshaber, E., Azmy, K., Buhl, D., 2011. What is the ideal proxy of Paleozoic seawater? The Association of Australasian Palaeontologists, Memoir 41, 9–24.

Brand, U., Posenato, R., Came, R., Affek, H., Angiolini, L., Azmy, K., Farabegoli, E., 2012. The end-Permian mass extinction: a rapid volcanic CO2 and CH4 -climatic catastrophe. Chemical Geology, 322-323: 121-144.

Brennecka, G.A., Herrmanna, A.D., Algeo, T.J., Anbara, A.D., 2011. Rapid expansion of oceanic anoxia immediately before the end-Permian mass extinction. Proceedings of the National Academy of Sciences USA 108 (43), 17631–17634.

Cawood, P.A., McCausland, P.J.A., Dunning, G.R., 2001. Opening Iapetus: Constraints from Laurentian margin in Newfoundland. Geological Society of America Bulletin 113, 443–453.

Cooper, R.A., Nowlan, G.S., Williams, S.H., 2001. Global Stratotype Section and Point for base of the Ordovician System. Episodes 24, 19–28.

Çoban-Yıldız, Y., Altabet, M.A., Yılmaz, A., Tuğrul, S., 2006. Carbon and nitrogen isotopic ratios of suspended particulate organic matter (SPOM) in the Black Sea water column. Deep-Sea Res. II 53, 1875–1892.

Condon, D.J., McLean, N., Noble, S.R., Bowring, S.A., 2010. Isotopic composition (U-238/U-235) of some commonly used uranium reference materials. Geochim. Cosmochim. Acta 74 (24), 7127–7143.

Dahl, T.W., Boyle, R.A., Canfield, D.E., Connelly, J.N., Gill, B.C., Lenton, T.M., Bizzarro, M., 2014. Uranium isotopes distinguish two geochemically distinct stages during the later Cambrian SPICE event. Earth Planet. Sci. Lett. 401, 313-326.

Davies, N.S., Gibling, M.R., 2010. Cambrian to Devonian evolution of alluvial systems: The sedimentological impact of the earliest land plants. Earth Science Reviews 98, 171-200.

Dickson, A.J., Cohen, A.S., Coe, A.L., 2011. Seawater oxygenation during the Paleocene-Eocene Thermal Maximum. Geology 40 (7), 639–642.

Dickson, J.A.D., 1966. Carbonate identification and genesis as revealed by staining. J. Sed. Petrol. 36, 491-505.

Dunk, R.M., Mills, R.A., Jenkins, W.J., 2002. A reevaluation of the oceanic uranium budget for the Holocene. Chem. Geol. 190, 45-67.

Falkowski, P.G., 2004. Biogeochemistry of primary production in the sea. *In*: Elderfield, H., Holland, H.D., Turekian, K.K. (Eds.), Biogeochemistry, Treatise on Geochemistry, v. 8. Elsevier, Amsterdam, Heidelberg, pp. 185–213.

Faure, G.; Mensing, T.M., 2005. Isotopes: principles and applications, third edition, John Willey and Sons, Inc., Hoboken, New Jersey, 897pp.

Fry, B., Jannasch, H.W., Molyneaux, S.J.,Wirsen, C.O., Muramoto, J.A., King, S., 1991. Stable isotope studies of the carbon, nitrogen and sulfur cycles in the Black Sea and the Cariaco Trench. Deep-Sea Res. 38, S1003–S1019.

Galbraith, E.D., Sigman, D.M., Robinson, R.S., Pedersen., T.F., 2008. "Nitrogen in past marine environments", In: Capone, D.G., Bronk, D.A., Mulholland, M.R., Carpenter, E.J. (Eds.), Nitrogen in the Marine Environment, 2nd edition. Academic Press, pp. 1497–1535. Chapter 34.

Halverson, G.P., Hoffman, P.F., Schrag, D.P., Maloof, A.C., Rice, A.H.N., 2005. Toward a Neoproterozoic composite carbon–isotope record. Geological Society of America Bulletin 117, 1181–1207.

Hatch, J.R., Leventhal, J.S., 1992. Relationship between inferred redox potential of the depositional environment and geochemistry of the Upper Pennsylvanian (Missourian) Stark Shale Member of the Dennis Limestone, Wabaunsee Country, Kansas, U.S.A. Chemical Geology 99, 65–82.

Helz, G.R., Vorlicek, T.P., Kahn, M.D., 2004. Molybdenum scavenging by iron monosulfide. Environ. Sci. Technol. 38, 4263–4268.

Hibbard, J.P., van Staal, C.R. and Ranking, D.G., 2007. A comparative analysis of pre-Silurian crustal building blocks of the northern and southern Appalachian orogeny. American Journal of Science 307, 23–45.

Immenhauser, I., Holmden, C., Patterson, W.P., 2008. Interpreting the carbon–isotope record of ancient shallow epiric seas: lessons from the Recent. In: Pratt B.R., Holmden, C. (Eds.), Dynamics of epeiric seas, Geological Association of Canada, Special Paper 48, 137–174.

James, N.P., Stevens, P.K., 1986. Stratigraphy and correlation of the Cambro–Ordovician Cow Head Group, western Newfoundland. Geological Survey of Canada Bulletin 366, 1–143.

James, N.P., Stevens, R.K., Barnes, C.R., Knight, I., 1989. Evolution of a Lower Paleozoic continental–margin carbonate platform, northern Canadian Appalachians In: Crevello, P. D. Wilson, J. L. Sarg, J. F. Read, J. F. (eds.), Controls on Carbonate Platform and Basin Development, Society of Economic Paleontologists and Mineralogists Special Publication 44, 123–146.

Kendall, B., Brennecka, G.A., Weyer, S., Anbar, A.D., 2013. Uranium isotope fractionation suggests oxidative uranium mobilization at 2.50Ga. Chemical Geology 362, 105–114.

Kendall, B., Komiya, T., Lyons, T.W., Bates, S.M., Gordon, G.W., Romaniello, S.J., Jiang, G., Creaser, R.A., Xiao, S., McFadden, K., Sawaki, Y., Tahata, M., Shu, D., Han, J., Li, Y., Chu, X., Anbar, A.D., 2015. Uranium and molybdenum isotope evidence for an episode of widespread ocean oxygenation during the late Ediacaran Period. Geochim. Cosmochim. Acta 156, 173-193.

Kimura, H., Azmy, K., Yamamuro, M., Zhi–Wen, J., Cizdziel, J. V., 2005. Integrated stratigraphy of the Upper Proterozoic succession in Yunnan of South China: re-evaluation of global correlation and carbon cycle. Precambrin Research 138, 1–36.

Knight, I., Azmy, K., Boyce, D., Lavoie, D., 2008. Tremadocian carbonates of the lower St. George Group, Port au Port Peninsula, western Newfoundland: Lithostratigraphic setting of diagenetic, isotopic, and geochemistry studies. Current Research Newfoundland and Labrador Department of Natural Resources Geological Survey. Report 08–1, 1–43.

Knight, I., Azmy, K., Greene, M., Lavoie, D., 2007. Lithostratigraphic setting of diagenetic, isotopic, and geochemistry studies of Ibexian and Whiterockian carbonates of the St. George and Table Head groups in western Newfoundland. Current Research Newfoundland and Labrador Department of Natural Resources Geological Survey. Report 07–1, 55–84.

Ku, T.L., Knauss, K., Mathieu, G.G., 1977. Uranium in the open ocean: concentration and isotopic composition. Deep Sea Research 24, 1005-1017.

Landing, E., 2007. Ediacaran–Ordovician of east Laurentia—geologic setting and controls on deposition along the New York Promontory, p. 5–24. *In* E. Landing (ed.), Ediacaran–Ordovician of east Laurentia—S. W. Ford Memorial Volume. New York State Museum Bulletin 510, 93 p.

Landing, E., 2012. Time-specific black mudstones and global hyperwarming on the Cambrian–Ordovician slope and shelf of the Laurentia palaeocontinent. Palaeogeography, Palaeoclimatology, Palaeoecology 367–368, 256–272.

Landing, E. 2013. The Great American Carbonate Bank in northeast Laurentia: its births, deaths, and linkage to continental slope oxygenation (Early Cambrian–Late Ordovician). *In*: J. R. Derby, R. D. Fritz, S. A. Longacre, W. A. Morgan, and C. A. Sternbach (eds.), The Great American Carbonate Bank, essays in honor of James Lee Wilson. American Association of Petroleum Geologists Bulletin, Memoir 98, 451–492.

Landing, E., Geyer, G., Bartowski, K.E., 2002. Latest Early Cambrian small shelly fossils, trilobites, and Hatch Hill dysaerobic interval on the east Laurentian continental slope. Journal of Paleontology 76, 285–303.

Landing, E., Keppie, J.D., Westrop, S.R., 2007. Terminal Cambrian and lowest Ordovician of Mexican West Gondwana—biotas and sequence stratigraphy of the Tiñu Formation. Geological Magazine 144, 909–936.

Lavoie, D., Desrochers, A., Dix, G., Knight, A. Hersi, O.S., 2013. The great carbonate Bank in eastern Canada: an overview. In: Derby, J., Fritz, R., Longcare, S., Morgan, W., Sternbach, C., (eds.), The Great American Carbonate Bank: the Geology and Economic Resources of Cambrian–Ordovician Sauk Megasequence of Laurentia. American Association of Petroleum Geologists, Memoir 98, 499–524.

Lécuyer, C., Grandjean, P., Barrat, J.-A., Nolvak, J., Emig, C., Paris, F., Robardet, M., 1998. $\delta^{18}O$ and REE contents of phosphatic brachiopods: a comparison between modern and lower Paleozoic populations. Geochimica et Cosmochimica Acta 62, 2429–2436.

Lehnert, O., Miller, J.F., Leslie, S.A., Repetski, J.E., Ethington, R.L., 2005. Cambro-Ordovician sea-level fluctuations and sequence boundaries: the missing record and evolution of new taxa. Special Papers in Palaeontology 73, 117–134.

Machel, H.G., Burton, E.A., 1991. Factors governing cathodoluminescence in calcite and dolomite, and their implications for studies of carbonate diagenesis. In: Luminescence microscopy and spectroscopy, qualitative and quantitative applications, SEPM Short Course 25, 37–57.

Meyers, P.A., 1994. Preservation of elemental and isotopic source identification of sedimentary organic matter. Chem. Geol. 144, 289–302.

Montoya-Pino, C., Weyer, S., Anbar, A.D., Pross, J., Oschmann, W., van de Schootbrugge, B., Arz, H.W., 2010. Global enhancement of ocean anoxia during Oceanic Anoxic Event 2: a quantitative approach using U isotopes. Geology 38:315–318.

Morel, F.M.M., Milligan, A.J., Saito, M.A., 2004. Marine bioinorganic chemistry: the role of trace metals in the oceanic cycles of major nutrients. In: Elderfield, H., Holland, H.D., Turekian, K.K. (Eds.), The Oceans and Marine Geochemistry, Treatise on geochemistry, volume 6. Elsevier, Amsterdam, Heidelberg, pp. 113–143.

Murphy, A.E., Sageman, B.B., Hollander, D.J., Lyons, D.J., Brett, C.E., 2000. Black shale deposition and faunal overturn in the Devonian Appalachian basin: clastic starvation, seasonal water-column mixing, and efficient biolimiting nutrient recycling. Paleoceanography 15, 280–291.

Partin, C.A., Bekker, A., Planavsky, N.J., Scott, C.T., Gill, B.C., Li, C., Podkovyrov, V., Maslov, A., Konhauser, K.O., Lalonde, S.V., Love, G.D., Poultonk, S.W., Lyons, T.W., 2013. Large-scale fluctuations in Precambrian atmospheric and oceanic oxygen levels from the record of U in shales. EPSL 369-370, 284-293.

Piper, D.Z., Calvert, S.E., 2009. A marine biogeochemical perspective on black shale deposition. Earth-Science Reviews 95, 63–96.

Popp, B.N., Parekh, P., Tilbrook, B., Bidigare, R.R., Laws, E.A., 1997. Organic carbon $\delta^{13}C$ variations in sedimentary rocks as chemostratigraphic and paleoenvironmental tools. Palaeogeography, Palaeoclimatology, Palaeoecology 132, 119–132.

Pouille, L., Danelian, T., Maletz, J., 2014. Radiolarian diversity changes during the Late Cambrian–Early Ordovician transition as recorded in the Cow Head Group of Newfoundland (Canada). Marine Micropaleontology 110, 25-41.

Poulson, R.L., Siebert, C., McManus, J., Berelson, W.M., 2006. Authigenic molybdenum isotope signatures in marine sediments. Geology 34, 617–620.

Quan, T.M., van de Schootbrugge, B., Field, M.P., Rosenthal, Y., Falkowski, P.G., 2008. Nitrogen isotope and trace metal analyses from the Mingolsheim core (Germany): evidence for redox variations across the Triassic–Jurassic boundary. Glob. Biogeochem. Cycles 22, GB2014.

Quan, T.M.,Wright, J.D., Falkowski, P.G., 2013. Co-variation of nitrogen isotopes and redo states through glacial–interglacial cycles in the Black Sea. Geochim. Cosmochim. Acta 112, 305–320.

Romaniello, S.J., 2013. Incorporation and Preservation of Molybdenum and Uranium Isotope Variations in Modern Marine Sediments. PhD Thesis, Arizona State University, 143pp.

Romaniello, S.J., Herrmann , A.D., Anbar, A.D., 2013. Uranium concentrations and $^{238}U/^{235}U$ isotope ratios in modern carbonates from the Bahamas: Assessing a novel paleoredox proxy. Chemical Geology 362, 305−316.

Rush, P.F., Chafetz, H.S., 1990. Fabric retentive, non–luminescent brachiopods as indicators of original $\delta^{13}C$ and $\delta^{18}O$ compositions: a test. Journal of Sedimentary Petrology 60, 968–981.

Scheiderich, K., Helz, G.R., Walker, R.J., 2010. Century-long record of Mo isotopic composition in sediments of a seasonally anoxic estuary (Chesapeake Bay). Earth Planet. Sci. Lett. 289, 189–197.

Śliwiński, M.G., Whalen, M.T., Day, J., 2010. Trace element variations in the Middle Frasnian punctata zone (Late Devonian) in the western Canada sedimentary Basin–changes in oceanic bioproductivity and paleoredox spurred by a pulse of terrestrial afforestation? Geologica Belgica 4, 459–482.

Telus, M., Dauphas, N., Moynier, F., Tissot, F.L.H., Teng, F.-Z., Nabelek, P.I., Craddock, P.R., Groat, L.A., 2012. Iron, zinc, magnesium and uranium isotopic fractionation during continental crust differentiation: the tale from migmatites, granitoids, and pegmatites. Geochimica et Cosmochimica Acta 97, 247–265.

Terfelt, F., Bagnoli, G., Stouge, S., 2102. Re-evaluation of the conodont *Iapetognathus* and implications for the base of the Ordovician System GSSP. Lethaia 45, 227–237.

Terfelt, F., Eriksson, M.E., Schmitz, B., 2014. The Cambrian–Ordovician transition in dysoxic facies in Baltica—diverse faunas and carbon isotope anomalies. Palaeo3 394, 59-73.

Theissen, K.M., Dunbar, R.B., Cooper, A.K., 2003. Stable isotopic measurements of sedimentary organic matter and *N. Pachyderma* (S.) from Site 1166, Prydz Bay continental shelf. In: Cooper, A.K., O'Brien, P.E., and Richter, C. (eds.). Proceedings of the Ocean Drilling Program, Scientific Results 188, 1− 11.

Tribovillard, N., Algeo, T.J., Lyons, T., Riboulleau, A., 2006. Trace metals as paleoredox and paleoproductivity proxies: An update. Chemical Geology 232, 12-32.

Tribovillard, N., Algeo, T.J., Baudin, F., Riboulleau, A., 2012. Analysis of marine environmental conditions based on molybdenum–uranium covariation—Applications to Mesozoic paleoceanography. Chemical Geology 324−325, 46−58.

Veizer, J. 1983. Chemical diagenesis of carbonates. In: Arthur, M.A., Anderson, T.F., Kaplan, I. R., Veizer, J., Land, L.S. (eds.), Theory and application of trace element technique, Stable Isotopes in Sedimentary Geology. Society of Economic Paleontologists and Mineralogists (SEPM) Short Course Notes 10, III–1–III–100.

687 Veizer, J., Ala, D., Azmy, K.; Bruckschen, P., Bruhn, F, Buhl, D. Carden, G., Diener, A.,
688 Ebneth, S., Goddris, Y., Jasper, T., Korte, C., Pawellek, F., Podlaha, O., Strauss, H., 1999.
689 $^{87}Sr/^{86}Sr$, $\delta^{18}O$ and $\delta^{13}C$ evolution of Phanerozoic seawater. Chemical Geology 161, 59–88.

690 Verbruggen, A., Alonso, A., Eykens, R., Kehoe, F., Kuhn, H., Richter, S., Aregbe, Y., 2008,
691 Preparation and certification of IRMM-3636, IRMM-3636a, and IRMM-3636b, Institute for
692 Reference Materials and Measurements, 27 p.

693 Weaver, F.J., Macko, S.A., 1988. Source rocks of western Newfoundland. Organic Chemistry 13
694 (1-3), 411−421.

695 Webb, G.E., Kamber, B.S., 2000. Rare Earth elements in Holocene reefal microbialites: a new
696 shallow seawater proxy. Geochimica et Cosmochimica Acta 64 (9), 1557–1565.

697 Westermann, S., Vance, D., Cameron, V., Archer, c., Robinson, S.A., 2014. Heterogeneous
698 oxygenation states in the Atlantic and Tethys oceans during Oceanic Anoxic Event 2. Earth and
699 Planet. Sci. Lett. 404, 178-189.

700 Weyer, S., Anbar, A.D., Gerdes, A., Gordon, G.W., Algeo, T.J., Boyle, E.A., 2008. Natural
701 fractionation of $^{238}U/^{235}U$. Geochim. Cosmochim. Acta72, 345–359.

702 Wignall, P.B., Twitchett, R.J., 1996. Oceanic anoxia and the end Permian mass extinction.
703 Science 272, 1155–1158.

704 Wignall, P.B., Zonneveld, J.-P., Newton, R.J., Amor, K., Sephton, M.A., Hartley, S., 2007. The
705 end Triassic mass extinction record of Williston Lake, British Columbia, Palaeogeography,
706 Palaeoclimatology, Palaeoecology 253, 385–406.

707 Wilson, J.L., Medlock, P.L., Fritz, R.D., Canter, K.L., Geesaman, R.G., 1992. A review of
708 Cambro–Ordovician breccias in North America, *In*: M. P. Candelaria and C. L. Reed, eds.,
709 Paleokarst, karst–related diagenesis and reservoir development. SEPM–Permian Basin Section,
710 Publication 92–33, 19–29.

711 Yamaguchi, K.E., Ogurim, K., Ogawa, N.O., Sakai, S., Hirano, S., Kitazato, H., Ohkouchi, N.,
712 2010. Geochemistry of modern carbonaceous sediments overlain by a water mass showing
713 photic zone anoxia in the saline meromictic Lake Kai-ike, southwest Japan: I. Early diagenesis of
714 organic carbon, nitrogen, and phosphorus. Palaeogeography, Palaeoclimatology, Palaeoecology
715 294, 72–82.

716 Zhou, L., Wignall, P.B., Su, J., Feng, Q., Xie, S., Zhao, L., Huang, J., 2012. U/Mo ratios and
717 $\delta^{95}/^{95}Mo$ as local and global redox proxies during mass extinction events. Chemical Geology
718 324−325, 99−107.

719

720 **List of Figures and Tables**

721 **Fig. 1**. Location map of Green Point, western Newfoundland, Canada (after Azmy et al., 2014)
722 showing (A) the location of the GSSP Cambrian–Ordovician boundary section in eastern
723 Canada, and (B) the distribution of outcrops of the beds covering the boundary interval
724 (modified from Cooper et al., 2001), and (C) the position of the GSSP on the paleomap during
725 the Cambrian–Ordovician time interval (based on Scotese, C. R., 2002, PALEOMAP
726 Project, http://www.scotese.com).

727 **Fig. 2**. Stratigraphic framework of the investigated Cambrian–Ordovician GSSP boundary
728 section in western Newfoundland, Canada showing the detailed measured section with the
729 positions of investigated samples and reconstructed sealevel variations across the boundary.
730 Conodont zonation after Landing et al. (2007). Abbreviations as follow: HST - high stand
731 systems tract, LST - low stand systems tract, TST - transgressive systems tract, MRS - maximum
732 regressive surface, MFS - maximum flooding surface, and SQB - sequence boundary.

733 **Fig. 3.** Photomicrographs of the investigated carbonates showing, (a) micritic lime mudstones
734 (Sample GP 21) and (b) CL image of (a).

735 **Fig. 4.** The $\delta^{13}C_{org}$, TOC, $\delta^{15}N_{org}$, and $\delta^{238}U$ profiles of lime mudstone rhythmites across the
736 Cambrian–Ordovician GSSP boundary section. The $\delta^{13}C_{carb}$ is reproduced from Azmy et al.
737 (2014). The solid grey line refers to the level of the geochemical anomaly recorded by Azmy et
738 al. (2014) and the dashed black line marks the current position of the Cambrian–Ordovician
739 boundary defined by the FAD of *I. fluctivagus* (Cooper et al., 2001). The dashed vertical red
740 lines are the mean values below and above the geochemical anomaly level.

741 **Fig. 5.** Scatter diagrams of (a) $\delta^{13}C_{org}$ vs. TOC and (b) $\delta^{15}N_{org}$ vs. TOC showing insignificant
742 correlations. Detail in text.

743 **Fig. 6.** Scatter diagram showing the correlations of Ce/Ce* vs. Y/Ho for the investigated
744 carbonates. $Ce_{SN}$ [$(Ce/Ce^*)_{SN} = Ce_{SN}/(0.5La_{SN}+0.5Pr_{SN})$] and $La_{SN}$ [$(Pr/Pr^*)_{SN} =$
745 $Pr_{SN}/0.5Ce_{SN}+0.5Nd_{SN})$] anomalies were calculated with the equations of Bau and Dulski (1996).
746 The grey square represents the composition of Holocene microbialites (Webb and Kamber,
747 2000).

748 **Fig. 7.** Scatter diagrams of Sr vs. (a) $\delta^{238}U$, (b) U showing insignificant correlations, and (c) U
749 vs. $\delta^{238}U$. Detail in text.

750 **Table 1.** Summary of statistics of GSSP geochemical results.

751 **Appendix 1.** Elemental and isotopic geochemical compositions of Green Point carbonates.
752 Concentrations of elements are in ppm and all values preceded by the sign "<" are below the
753 detection limit. The column "*n*" refers to the number of $\delta^{238}U$ measurements for each sample (rpt
754 = replicate sample).

755

756

757

758

759

**Figure 1**

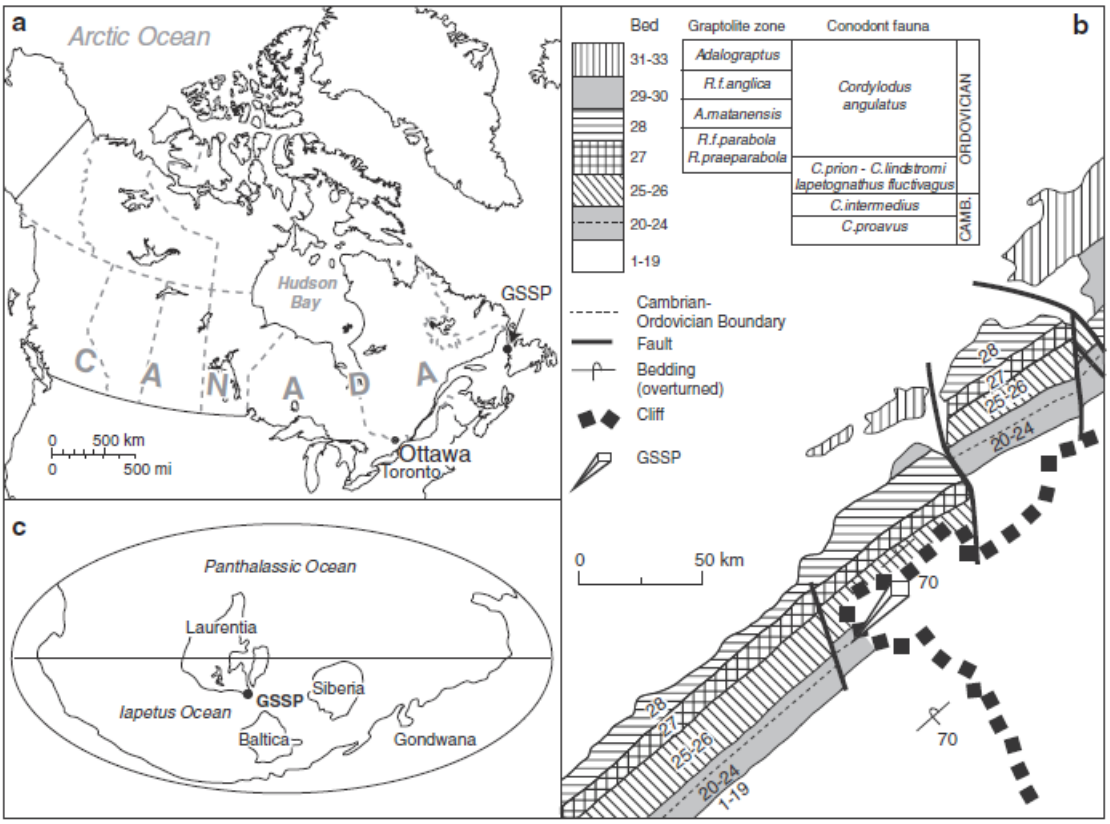
a
Arctic Ocean
Hudson Bay
GSSP
CANADA
0 500 km
0 500 mi
Ottawa
Toronto
c
Panthalassic Ocean
Laurentia
GSSP
Siberia
Iapetus Ocean
Baltica
Gondwana
b
Bed
Graptolite zone
Conodont fauna
31-33
29-30
28
27
25-26
20-24
1-19
Adalograptus
R.f.anglica
A.matanensis
R.f.parabola
R.praeparabola
Cordylodus angulatus
C.prion - C.lindstromi
Iapetognathus fluctivagus
C.intermedius
C.proavus
ORDOVICIAN
CAMB.
Cambrian-Ordovician Boundary
Fault
Bedding (overturned)
Cliff
GSSP
0 50 km
70
70

769 **Figure 2**

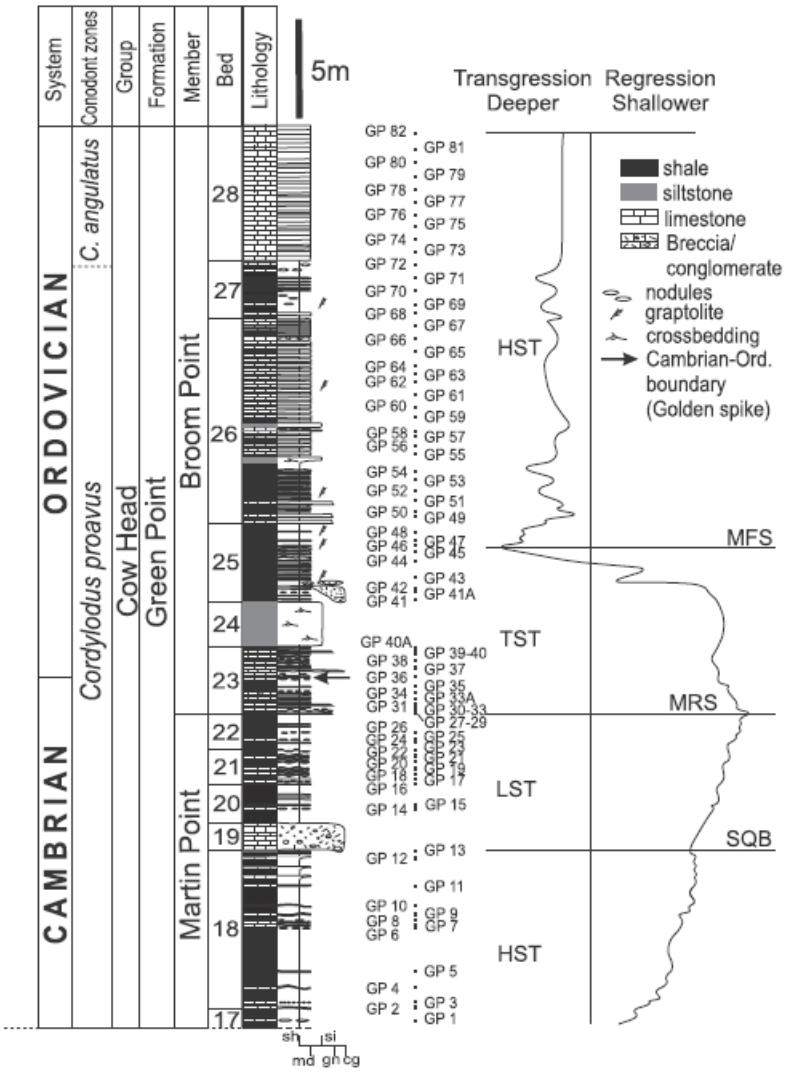


770

771

772

773

774

775

776 **Figure 3**

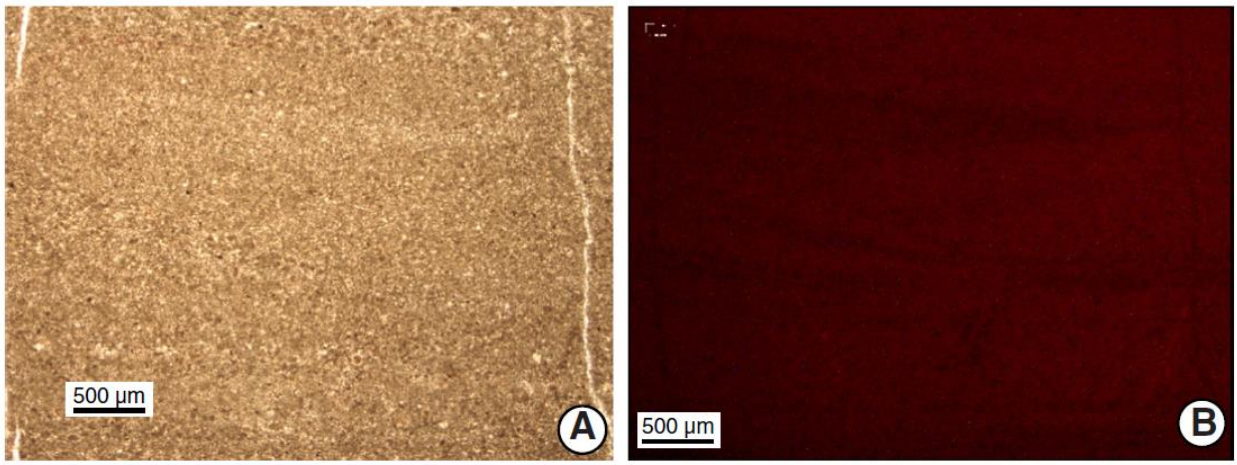


777

778

779

780

781

782

783

784

785

786

787

788

**Figure 4**

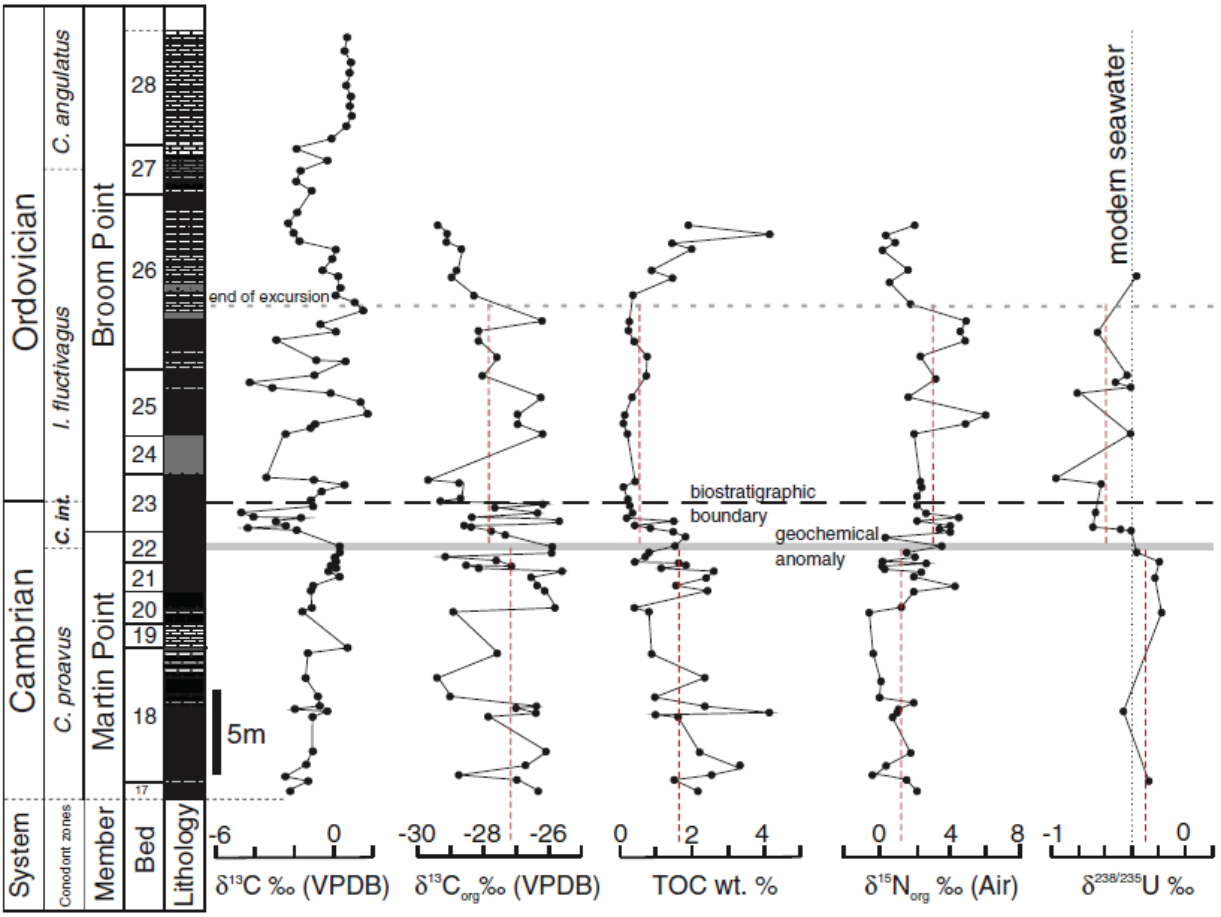
System
Cambrian
Ordovician
Conodont zones
C. proavus
C. int.
I. fluctivagus
C. angulatus
Member
Martin Point
Broom Point
Bed
Lithology
17
18
19
20
21
22
23
24
25
26
27
28
5m
end of excursion
biostratigraphic boundary
geochemical anomaly
modern seawater
-6
0
δ13C ‰ (VPDB)
-30
-28
-26
δ13Corg‰ (VPDB)
0
2
4
TOC wt. %
0
4
8
δ15Norg ‰ (Air)
-1
0
δ238/235U ‰

797 **Figure 5**

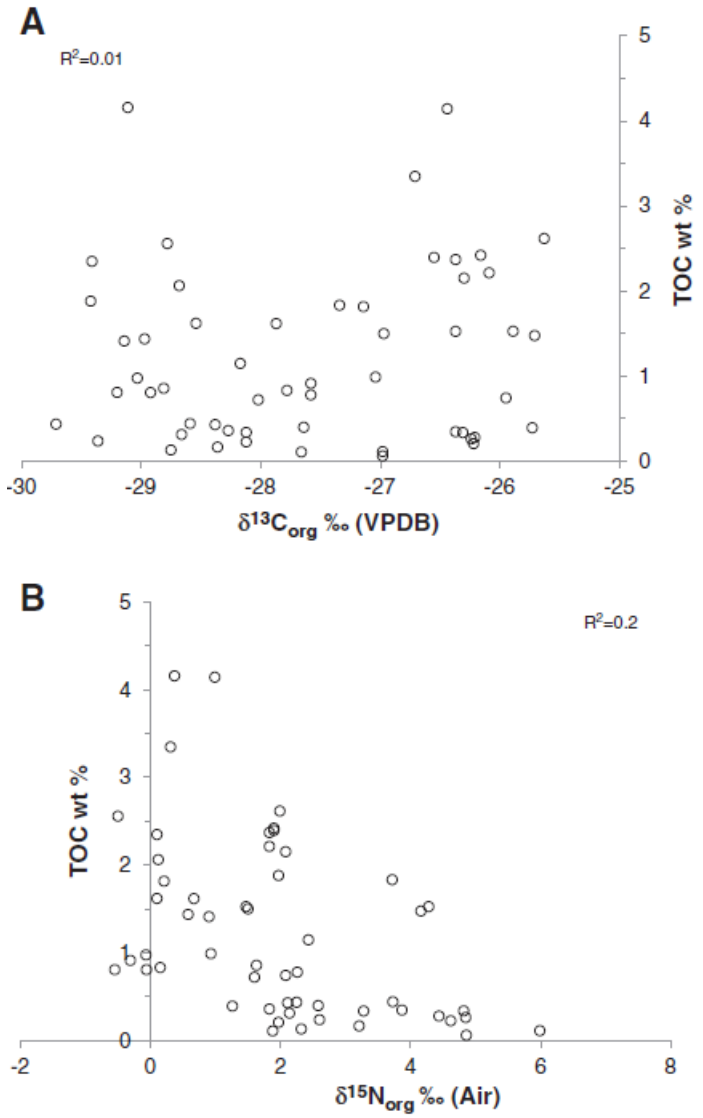


798

799

800

801

802

803 **Figure 6**

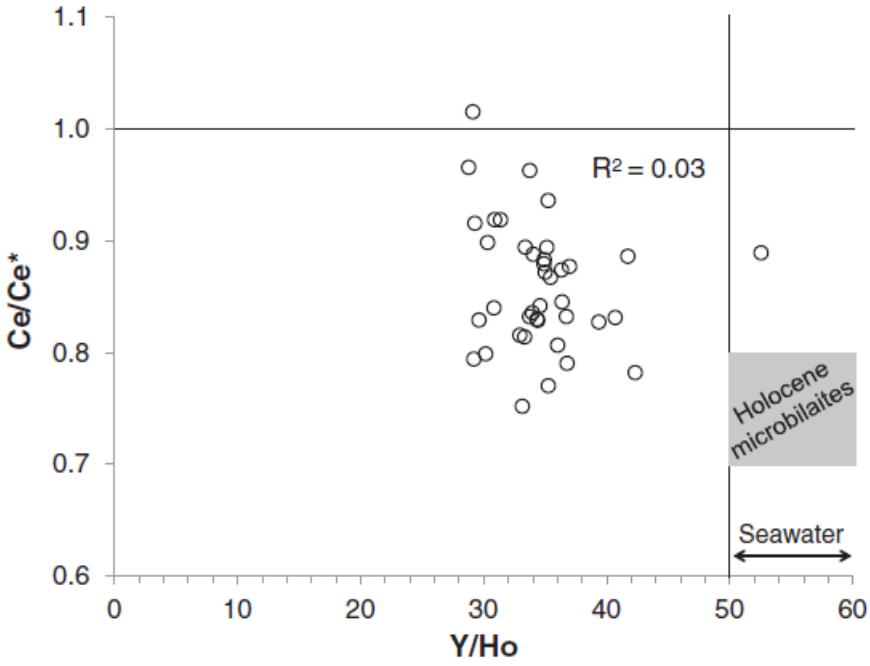


804

805

806

807

808

809

810

811

812

**Figure 7**

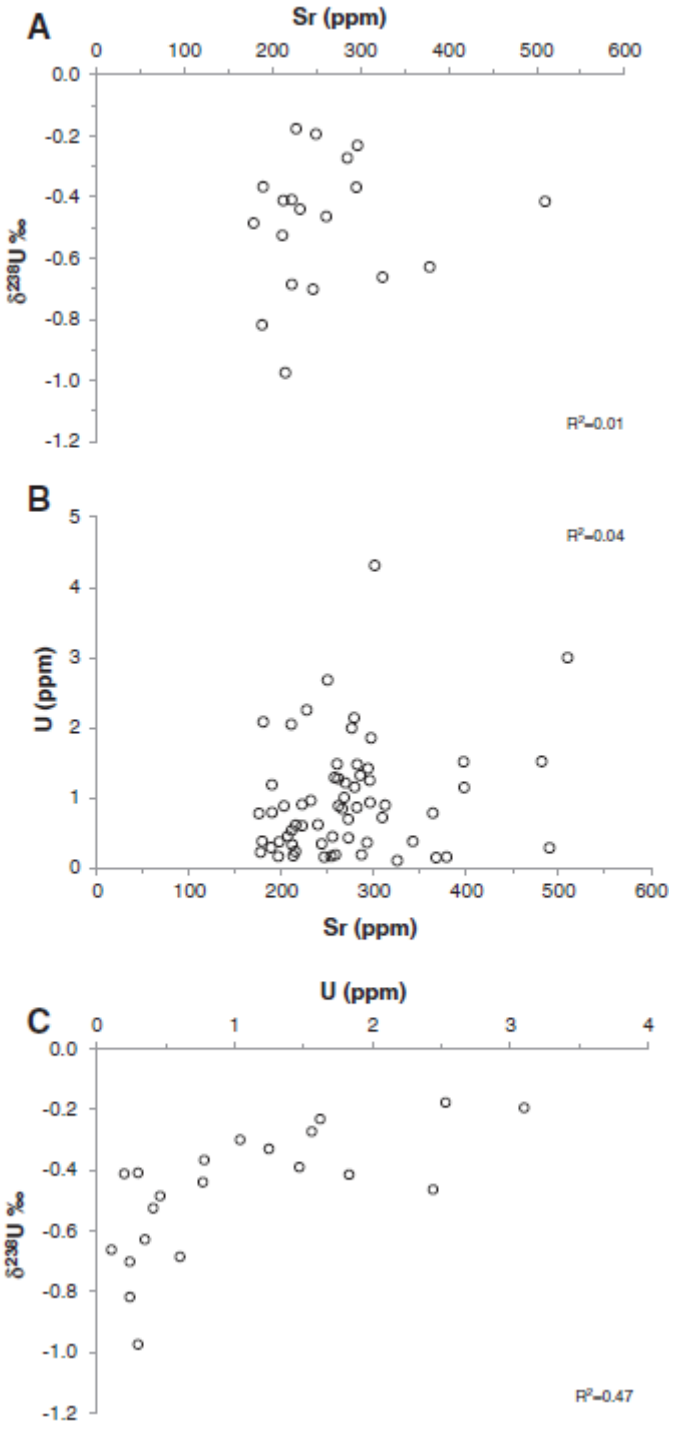
A
Sr (ppm)
0
100
200
300
400
500
600
0.0
-0.2
-0.4
-0.6
-0.8
-1.0
-1.2
δ238U ‰
R²=0.01
B
R²=0.04
U (ppm)
0
1
2
3
4
5
Sr (ppm)
C
U (ppm)
δ238U ‰
R²=0.47

816 **Table 1**

| | | $\delta^{13}C_{org}$ | % TOC | $\delta^{15}N_{air}$ | % N | $\delta^{238}U$ | U (ppm) | Th/U |
|---|---|---|---|---|---|---|---|---|
| *n* | Above geochem anomaly (Sample Gp26) | 26 | 26 | 27 | 26 | 13 | 36 | 15 |
| Average | | −27.8 | 0.6 | 2.8 | 0.33 | −0.58 | 0.7 | 0.7 |
| Stdev | | 1.1 | 0.5 | 1.5 | 0.62 | 0.18 | 0.7 | 0.5 |
| Max | | −25.7 | 2.1 | 6.0 | 2.91 | −0.37 | 3.0 | 1.7 |
| Min | | −29.7 | 0.1 | 0.1 | 0.00 | −0.97 | 0.1 | 0.2 |
| *n* | Below geochem anomaly (Sample Gp26) | 25 | 25 | 25 | 25 | 6 | 26 | 24 |
| Average | | −27.2 | 1.7 | 1.2 | 0.01 | −0.28 | 1.2 | 0.5 |
| Stdev | | 1.2 | 0.9 | 1.2 | 0.01 | 0.11 | 0.6 | 0.4 |
| Max | | −25.6 | 4.1 | 4.3 | 0.06 | −0.18 | 2.7 | 1.7 |
| Min | | −29.4 | 0.4 | −0.6 | 0.00 | −0.46 | 0.3 | 0.1 |
| *n* | Entire section | 51 | 51 | 52 | 51 | 19 | 62 | 39 |
| Average | | −27.5 | 1.1 | 2.0 | 0.17 | −0.47 | 1.0 | 0.6 |
| Stdev | | 1.2 | 1.0 | 1.6 | 0.47 | 0.21 | 0.8 | 0.4 |
| Max | | −25.6 | 4.1 | 6.0 | 2.91 | −0.18 | 4.3 | 1.7 |
| Min | | −29.7 | 0.1 | −0.6 | 0.00 | −0.97 | 0.1 | 0.1 |

817

818

819

820

821

822

823

824

825

826

827

828

829

# Appendix 1

| Sample id # | $\delta^{13}C_{carb}$ ‰ | $\delta^{18}O$ ‰ | $\delta^{13}C_{org}$ ‰ | %TOC | $\delta^{15}N_{tot}$ ‰ | %N | $\delta^{238}/^{235}U$ ‰ | ±2σ | $\delta^{234}/^{238}U$ ‰ | ±2σ | n | $CaCO_3$% | $MgCO_3$% | Al | Si | Ti | V | Cr | Mn | Sr |
|---|---|---|---|---|---|---|---|---|---|---|---|---|---|---|---|---|---|---|---|---|
| GP 1 | −2.26 | −7.34 | −26.30 | 2.15 | 2.08 | 0.004 | | | | | | 97.8 | 2.2 | 1539 | 2586 | 33 | 5 | 2 | 746 | 312 |
| GP 2 | −1.29 | −7.21 | −26.97 | 1.50 | 1.50 | 0.003 | −0.27 | 0.04 | 1.9 | 1.7 | 4 | 98.7 | 1.3 | 372 | 648 | 19 | 1 | 1 | 800 | 285 |
| GP 2rpt | | | | | | | −0.30 | 0.09 | 5.3 | 7.9 | 2 | | | | | | | | | |
| GP 3 | −2.37 | −7.22 | −28.78 | 2.56 | −0.50 | 0.061 | | | | | | 98.5 | 1.5 | 1043 | 1855 | 37 | 4 | 2 | 499 | 215 |
| GP 4 | −1.39 | −7.09 | −26.71 | 3.35 | 0.31 | 0.002 | | | | | | 98.8 | 1.2 | 540 | 927 | 17 | 2 | 1 | 531 | 301 |
| GP 5 | −1.10 | −7.25 | −26.09 | 2.21 | 1.83 | 0.003 | | | | | | 97.9 | 2.1 | 1328 | 1903 | 27 | 3 | 1 | 489 | 296 |
| GP 6 | −1.07 | −7.11 | −27.87 | 1.62 | 0.67 | 0.005 | | | | | | 98.8 | 1.2 | 492 | 802 | 18 | 2 | 1 | 315 | 260 |
| GP 7 | −0.32 | −6.89 | −26.44 | 4.14 | 0.99 | 0.003 | −0.46 | 0.05 | 0.8 | 5.5 | 3 | 98.8 | 1.2 | 520 | 858 | 20 | 2 | 1 | 346 | 261 |
| GP 8 | −2.01 | −7.72 | −27.04 | 0.99 | 0.93 | 0.007 | | | | | | 97.0 | 3.0 | 1935 | 2922 | 48 | 7 | 3 | 483 | 294 |
| GP 9 | −0.67 | −7.08 | −26.37 | 2.37 | 1.83 | 0.003 | | | | | | 98.7 | 1.3 | 568 | 1146 | 24 | 2 | 2 | 389 | 266 |
| GP 10 | −0.81 | −7.56 | −29.03 | 0.97 | −0.07 | 0.011 | | | | | | 98.8 | 1.2 | 633 | 1045 | 18 | 1 | 1 | 579 | 239 |
| GP 11 | −1.49 | −5.63 | −29.41 | 2.35 | 0.10 | 0.048 | | | | | | 62.0 | 38.0 | 11,754 | 17,706 | 314 | 176 | 23 | 1054 | 279 |
| GP 12 | −1.32 | −5.52 | −27.58 | 0.91 | −0.31 | 0.008 | | | | | | 63.8 | 36.2 | 4902 | 9331 | 106 | 34 | 8 | 985 | 206 |
| GP 13 | 0.75 | −6.87 | | | | | | | | | | 99.1 | 0.9 | 302 | 462 | 13 | 1 | 1 | 267 | 211 |
| GP 14 | −1.52 | −7.45 | −28.92 | 0.80 | −0.55 | 0.023 | −0.18 | 0.08 | 28.2 | 5.2 | 4 | 98.7 | 1.3 | 878 | 1366 | 23 | 3 | 2 | 671 | 227 |
| GP 15 | −1.11 | −8.57 | −25.73 | 0.39 | 1.26 | 0.006 | | | | | | 98.0 | 2.0 | 3162 | 6529 | 86 | 4 | 4 | 331 | 490 |
| GP 16 | −1.20 | −8.53 | −26.16 | 2.42 | 1.90 | 0.004 | | | | | | 99.0 | 1.0 | 647 | 1117 | 12 | 4 | 1 | 282 | 364 |
| GP 17 | −1.07 | −7.06 | −26.37 | 1.52 | 4.28 | 0.003 | | | | | | 98.6 | 1.4 | 1102 | 1778 | 30 | 3 | 2 | 684 | 210 |
| GP 18 | 0.36 | −6.98 | −26.55 | 2.39 | 1.90 | 0.005 | −0.23 | | 5.3 | | 1 | 98.7 | 1.3 | 640 | 999 | 18 | 3 | 1 | 280 | 297 |
| GP 19 | −0.30 | −7.15 | −25.63 | 2.62 | 1.99 | 0.004 | | | | | | 98.8 | 1.2 | 687 | 1008 | 17 | 2 | 1 | 435 | 257 |
| GP 20 | 0.13 | −7.12 | −28.17 | 1.15 | 2.43 | 0.003 | | | | | | 98.8 | 1.2 | 483 | 879 | 20 | 1 | 1 | 371 | 272 |
| GP 21 | 0.03 | −6.98 | −27.14 | 1.81 | 0.21 | 0.013 | | | | | | 98.8 | 1.2 | 489 | 858 | 19 | 2 | 1 | 396 | 276 |
| GP 22 | −0.18 | −7.09 | −28.54 | 1.62 | 0.10 | 0.008 | −0.19 | 0.01 | −14.3 | 1.4 | 3 | 98.8 | 1.2 | 371 | 716 | 15 | 2 | 2 | 369 | 250 |
| GP 23 | 0.06 | −7.16 | −27.64 | 0.40 | 2.58 | 0.003 | | | | | | 98.5 | 1.5 | 692 | 1190 | 24 | 2 | 2 | 579 | 255 |
| GP 24 | 0.02 | −7.32 | −29.20 | 0.81 | −0.06 | 0.019 | | | | | | 98.5 | 1.5 | 614 | 1187 | 22 | 2 | 1 | 644 | 282 |
| GP 25 | 0.36 | −7.37 | −25.95 | 0.74 | 2.08 | 0.003 | −0.37 | | 9.8 | | 1 | 98.5 | 1.5 | 1083 | 2024 | 30 | 3 | 1 | 628 | 190 |
| GP 26 | 0.27 | −7.19 | −25.89 | 1.52 | 1.47 | 0.003 | | | | | | 97.6 | 2.4 | 1558 | 2712 | 37 | 3 | 2 | 558 | 175 |
| GP 27 | −2.05 | −8.65 | −27.34 | 1.83 | 3.72 | 0.021 | | | | | | 97.9 | 2.1 | 1785 | 3988 | 38 | 9 | 2 | 386 | 510 |
| GP 28 | −2.04 | −8.37 | −27.78 | 0.83 | 0.15 | 0.005 | −0.41 | 0.09 | 6.3 | 4.8 | 3 | 98.1 | 1.9 | 1104 | 2294 | 23 | 5 | 2 | 365 | 482 |
| GP 28rpt | | | | | | | −0.39 | 0.15 | 6.7 | 0.7 | 4 | | | | | | | | | |
| GP 29 | −4.40 | −7.38 | −28.38 | 0.43 | 2.11 | 0.007 | −0.49 | 0.10 | 14.6 | 5.7 | 4 | 98.7 | 1.3 | 766 | 1321 | 14 | 1 | 1 | 405 | 179 |
| GP 30 | −2.46 | −7.37 | −28.59 | 0.44 | 3.73 | 0.016 | −0.70 | 0.04 | 2.3 | 2.3 | 3 | 98.6 | 1.4 | 703 | 1267 | 15 | 2 | 1 | 376 | 246 |
| GP 31 | −2.75 | −7.40 | −25.71 | 1.47 | 4.16 | 0.004 | | | | | | 98.7 | 1.3 | 725 | 1259 | 14 | 1 | 1 | 339 | 196 |
| GP 32 | −3.00 | −8.02 | −28.36 | 0.16 | 3.21 | 2.914 | | | | | | 98.6 | 1.4 | 686 | 1158 | 14 | 1 | 1 | 460 | 258 |
| GP 33 | −1.45 | −8.04 | −26.37 | 0.34 | 3.87 | 0.641 | | | | | | 98.0 | 2.0 | 1571 | 3442 | 30 | 4 | 2 | 273 | 397 |
| GP 33A | −4.09 | −7.28 | −27.66 | 0.10 | 1.88 | 1.471 | | | | | | 98.5 | 1.5 | 1137 | 1761 | 15 | 2 | 1 | 338 | 197 |
| GP 34 | −4.72 | −6.98 | −26.21 | 0.27 | 4.44 | 0.107 | −0.69 | 0.12 | 11.2 | 2.1 | 4 | 98.5 | 1.5 | 920 | 1615 | 20 | 2 | 1 | 325 | 222 |
| GP 35 | −1.03 | −6.92 | −29.36 | 0.23 | 2.60 | 0.484 | | | | | | 98.4 | 1.6 | 1188 | 1724 | 25 | 9 | 1 | 474 | 180 |
| GP 36 | −1.22 | −7.03 | −28.66 | 0.31 | 2.14 | 0.585 | | | | | | 98.6 | 1.4 | 910 | 1384 | 29 | 4 | 1 | 249 | 203 |
| GP 37 | −0.62 | −6.84 | | | | | | | | | | 98.3 | 1.7 | 1142 | 1843 | 16 | 1 | 1 | 193 | 189 |
| GP 38 | 0.64 | −7.20 | −28.75 | 0.13 | 2.32 | 0.026 | −0.63 | 0.09 | 2.3 | 5.3 | 4 | 98.4 | 1.6 | 706 | 1225 | 21 | 1 | 1 | 122 | 379 |
| GP 39 | −1.05 | −8.04 | −29.71 | 0.43 | 2.25 | 0.232 | | | | | | 98.5 | 1.5 | 1010 | 1757 | 20 | 2 | 1 | 273 | 286 |

**Appendix 1.** (*continued*)

| Sample id # | $\delta^{13}C_{carb}$ ‰ | $\delta^{18}O$ ‰ | $\delta^{13}C_{org}$ ‰ | % TOC | $\delta^{15}N_{air}$ ‰ | % N | $\delta^{238}/^{235}U$ ‰ | ±2σ | $\delta^{234}/^{238}U$ ‰ | ±2σ | n | $CaCO_3$% | $MgCO_3$% | Al | Si | Ti | V | Cr | Mn | Sr |
|---|---|---|---|---|---|---|---|---|---|---|---|---|---|---|---|---|---|---|---|---|
| GP 40 | −3.42 | −7.44 | | | | | −0.97 | 0.15 | 7.9 | 6.3 | 4 | 98.7 | 1.3 | 745 | 1217 | 15 | 1 | 1 | 254 | 215 |
| GP 40 A | −1.30 | −7.29 | | | | | | | | | | | | | | | | | | |
| GP 41 | −2.57 | −7.17 | −26.22 | 0.20 | 1.97 | 0.064 | | | | | | 97.2 | 2.8 | 2010 | 3827 | 27 | 3 | 3 | 338 | 222 |
| GP 41 A | −1.18 | −7.11 | | | | | −0.41 | 0.02 | −2.5 | 3.7 | 3 | 98.7 | 1.3 | 579 | 1169 | <0.02 | 1 | 1 | 210 | 243 |
| GP 42 | −0.88 | −6.90 | −26.98 | 0.06 | 4.86 | 0.009 | | | | | | 98.9 | 1.1 | 496 | 1015 | <0.02 | 0 | 2 | 288 | 177 |
| GP 43 | 1.73 | −6.98 | −26.98 | 0.11 | 5.99 | 0.007 | | | | | | 98.2 | 1.8 | 671 | 1361 | 15 | 1 | 2 | 94 | 367 |
| GP 44 | 1.32 | −6.67 | | | 1.64 | | | | | | | 98.2 | 1.8 | 473 | 1094 | 17 | 1 | 2 | 90 | 342 |
| GP 45 | −0.21 | −6.86 | | | | | −0.82 | 0.02 | −7.3 | 0.9 | 3 | 98.8 | 1.2 | 427 | 884 | 12 | 1 | 1 | 824 | 189 |
| GP 46 | −3.03 | −6.83 | −26.31 | 0.33 | 3.28 | 0.003 | −0.41 | | −21.3 | | 1 | 98.8 | 1.2 | 286 | 520 | 9 | 1 | 2 | 834 | 213 |
| GP 47 | −4.26 | −6.91 | | | | | −0.53 | 0.06 | −9.4 | 3.0 | 3 | 98.6 | 1.4 | 644 | 1151 | 14 | 4 | 2 | 385 | 211 |
| GP 48 | −1.02 | −7.49 | −28.02 | 0.72 | 1.60 | 0.130 | −0.44 | 0.09 | 8.1 | 0.6 | 2 | 98.1 | 1.9 | 1371 | 2369 | 35 | 5 | 3 | 449 | 232 |
| GP 49 | −0.34 | −7.47 | | | | | | | | | | 98.6 | 1.4 | 230 | 453 | 5 | 2 | 5 | 213 | 398 |
| GP 50 | 0.56 | −7.55 | −27.58 | 0.78 | 2.26 | 0.380 | | | | | | 98.5 | 1.5 | 1064 | 1822 | 27 | 4 | 4 | 201 | 262 |
| GP 51 | −0.87 | −7.29 | | | | | | | | | | 98.5 | 1.5 | 1036 | 1727 | 32 | 4 | 4 | 149 | 272 |
| GP 52 | −2.86 | −7.76 | −28.12 | 0.33 | 4.82 | 0.048 | | | | | | 98.4 | 1.6 | 472 | | 16 | 2 | 2 | 178 | 293 |
| GP 53 | 0.17 | −6.91 | −28.12 | 0.22 | 4.62 | 0.093 | −0.66 | 0.11 | −20.8 | 1.7 | 4 | 98.7 | 1.3 | 406 | 666 | 16 | 2 | 2 | 128 | 325 |
| GP 54 | −0.75 | −8.12 | | | | | | | | | | 98.5 | 1.5 | 380 | 672 | 5 | 2 | 2 | 439 | 254 |
| GP 55 | 1.47 | −7.12 | −26.24 | 0.26 | 4.85 | 0.004 | | | | | | 98.7 | 1.3 | 783 | 1282 | 18 | 2 | 2 | 148 | 309 |
| GP 56 | 1.06 | −7.40 | | | | | | | | | | 98.8 | 1.2 | 532 | 973 | 21 | 2 | 3 | 144 | 282 |
| GP 57 | 0.06 | −7.92 | −28.27 | 0.36 | 1.83 | 0.036 | | | | | | 98.8 | 1.2 | 677 | 1047 | 29 | 5 | 3 | 179 | 269 |
| GP 58 | 0.24 | −7.46 | | | | | | | | | | 98.8 | 1.2 | 611 | 1041 | 30 | 6 | 3 | 200 | 268 |
| GP 59 | 0.27 | −7.38 | −28.97 | 1.43 | 0.58 | 0.514 | −0.33 | 0.13 | 6.1 | 5.7 | 4 | 98.9 | 1.1 | 487 | 818 | 25 | 3 | 3 | 129 | 295 |
| GP 59rpt | | | | | | | −0.37 | 0.06 | 4.9 | 1.2 | 3 | | | | | | | | | |
| GP 60 | −0.57 | −7.60 | −28.81 | 0.85 | 1.63 | 0.204 | | | | | | 98.9 | 1.1 | 690 | 1288 | 39 | 10 | 4 | 138 | 279 |
| GP 61 | −0.07 | −7.70 | | | | | | | | | | | | | | | | | | |
| GP 62 | 0.07 | −7.94 | −28.68 | 2.06 | 0.12 | 0.627 | | | | | | | | | | | | | | |
| GP 63 | −1.76 | −7.84 | −29.14 | 1.41 | 0.90 | 0.469 | | | | | | | | | | | | | | |
| GP 64 | −2.04 | −7.81 | −29.11 | 4.16 | 0.37 | 3.557 | | | | | | | | | | | | | | |
| GP 65 | −2.25 | −7.21 | | | | | | | | | | | | | | | | | | |
| GP 66 | | | −29.42 | 1.88 | 1.97 | 1.667 | | | | | | | | | | | | | | |
| GP 67 | −1.83 | −7.72 | | | | | | | | | | | | | | | | | | |
| GP 68 | −1.06 | −7.88 | | | | | | | | | | | | | | | | | | |
| GP 69 | −1.92 | −7.42 | | | | | | | | | | | | | | | | | | |
| GP 70 | −1.71 | −7.42 | | | | | | | | | | | | | | | | | | |
| GP 71 | −0.33 | −7.21 | | | | | | | | | | | | | | | | | | |
| GP 72 | −1.92 | −7.88 | | | | | | | | | | | | | | | | | | |
| GP 73 | −0.12 | −7.72 | | | | | | | | | | | | | | | | | | |
| GP 74 | 0.60 | −7.78 | | | | | | | | | | | | | | | | | | |
| GP 75 | 0.81 | −7.76 | | | | | | | | | | | | | | | | | | |
| GP 76 | 0.80 | −7.79 | | | | | | | | | | | | | | | | | | |
| GP 77 | 0.85 | −7.77 | | | | | | | | | | | | | | | | | | |
| GP 78 | 0.66 | −7.84 | | | | | | | | | | | | | | | | | | |
| GP 79 | 0.78 | −7.85 | | | | | | | | | | | | | | | | | | |
| GP 80 | 0.83 | −7.61 | | | | | | | | | | | | | | | | | | |
| GP 81 | 0.57 | −7.82 | | | | | | | | | | | | | | | | | | |
| GP 82 | 0.65 | −7.78 | | | | | | | | | | | | | | | | | | |

**Appendix 1.** (*continued*)

| Sample id # | Co | Ni | Cu | Mo | P | Y | La | Ce | Pr | Nd | Sm | Eu | Gd | Tb | Dy | Ho | Er | Tm | Yb | Lu | Th | U | Th/U | Y/Ho |
|---|---|---|---|---|---|---|---|---|---|---|---|---|---|---|---|---|---|---|---|---|---|---|---|---|
| GP 1 | <0.001 | <0.004 | <0.003 | 0.10 | 209 | 10 | 15.699 | 27.167 | 2.932 | 11.027 | 1.802 | 0.446 | 2.011 | 0.292 | 1.506 | 0.309 | 0.872 | 0.113 | 0.720 | 0.108 | 0.779 | 0.897 | 0.87 | 31 |
| GP 2 | <0.001 | <0.004 | <0.003 | 0.17 | 141 | 6 | 8.174 | 14.288 | 1.404 | 5.311 | 0.880 | 0.233 | 1.096 | 0.149 | 0.794 | 0.169 | 0.486 | 0.058 | 0.392 | 0.059 | 0.339 | 1.560 | 0.26 | 34 |
| GP 2rpt | | | | | | | | | | | | | | | | | | | | | | 1.040 | | |
| GP 3 | <0.001 | <0.004 | <0.003 | 0.13 | 88 | 25 | 30.057 | 58.174 | 5.766 | 22.516 | 3.979 | 1.053 | 4.842 | 0.753 | 4.081 | 0.845 | 2.344 | 0.293 | 1.772 | 0.260 | 0.561 | 0.612 | 0.92 | 29 |
| GP 4 | <0.001 | <0.004 | <0.003 | 0.05 | 134 | 13 | 15.086 | 25.171 | 2.481 | 9.606 | 1.692 | 0.453 | 2.072 | 0.310 | 1.701 | 0.368 | 1.024 | 0.136 | 0.820 | 0.125 | 0.320 | 4.313 | 0.07 | 35 |
| GP 5 | <0.001 | <0.004 | <0.003 | 0.07 | 184 | 10 | 13.876 | 24.957 | 2.820 | 10.201 | 1.764 | 0.459 | 1.962 | 0.291 | 1.470 | 0.303 | 0.829 | 0.111 | 0.703 | 0.105 | 0.588 | 0.935 | 0.63 | 31 |
| GP 6 | <0.001 | <0.004 | <0.003 | 0.09 | 73 | 5 | 7.706 | 11.765 | 1.359 | 4.813 | 0.787 | 0.209 | 0.888 | 0.126 | 0.627 | 0.123 | 0.350 | 0.043 | 0.267 | 0.038 | 0.208 | 1.483 | 0.14 | 41 |
| GP 7 | <0.001 | <0.004 | <0.003 | 0.07 | 80 | 4 | 5.809 | 9.617 | 1.118 | 4.080 | 0.701 | 0.176 | 0.782 | 0.111 | 0.553 | 0.114 | 0.302 | 0.038 | 0.236 | 0.033 | 0.297 | 2.440 | 0.23 | 35 |
| GP 8 | <0.001 | <0.004 | <0.003 | 0.09 | 319 | 17 | 23.211 | 42.063 | 4.829 | 18.181 | 3.396 | 0.863 | 3.772 | 0.560 | 2.917 | 0.584 | 1.607 | 0.206 | 1.263 | 0.179 | 0.937 | 1.421 | 0.66 | 29 |
| GP 9 | <0.001 | <0.004 | 14 | 0.08 | 101 | 4 | 5.543 | 9.184 | 1.056 | 3.953 | 0.738 | 0.200 | 0.821 | 0.119 | 0.580 | 0.113 | 0.308 | 0.035 | 0.207 | 0.031 | 0.248 | 0.844 | 0.29 | 35 |
| GP 10 | <0.001 | <0.004 | <0.003 | 0.09 | 163 | 8 | 16.065 | 23.233 | 2.779 | 9.815 | 1.692 | 0.495 | 1.887 | 0.276 | 1.391 | 0.263 | 0.683 | 0.081 | 0.507 | 0.072 | 0.267 | 0.619 | 0.43 | 29 |
| GP 11 | 18 | 47 | 29 | | 868 | 7 | 12.687 | 27.001 | 3.412 | 13.090 | 2.403 | 0.541 | 2.385 | 0.331 | 1.571 | 0.298 | 0.774 | 0.092 | 0.565 | 0.080 | | | | |
| GP 12 | 46 | 5 | 6 | | 586 | 9 | 13.439 | 27.555 | 3.408 | 12.884 | 2.387 | 0.547 | 2.427 | 0.356 | 1.784 | 0.345 | 0.941 | 0.115 | 0.724 | 0.104 | | | | |
| GP 13 | <0.001 | <0.004 | <0.003 | 0.09 | 77 | 2 | 3.761 | 5.564 | 0.623 | 2.104 | 0.325 | 0.083 | 0.345 | 0.049 | 0.235 | 0.044 | 0.125 | 0.015 | 0.093 | 0.014 | 0.151 | 0.538 | 0.28 | 39 |
| GP 14 | <0.001 | <0.004 | <0.003 | 0.29 | 90 | 16 | 15.313 | 23.670 | 2.799 | 10.890 | 2.066 | 0.581 | 2.487 | 0.391 | 2.159 | 0.452 | 1.287 | 0.157 | 0.926 | 0.139 | 0.346 | 2.530 | 0.15 | 34 |
| GP 15 | 6 | <0.004 | <0.003 | 0.28 | 295 | 23 | 26.675 | 43.883 | 5.429 | 19.622 | 3.736 | 1.003 | 3.972 | 0.688 | 3.733 | 0.742 | 2.112 | 0.274 | 1.782 | 0.256 | 0.485 | 0.288 | 1.68 | 31 |
| GP 16 | <0.001 | <0.004 | <0.003 | 0.96 | 674 | 34 | 41.762 | 68.584 | 9.009 | 34.280 | 6.612 | 1.823 | 7.135 | 1.119 | 5.488 | 1.042 | 2.696 | 0.308 | 1.886 | 0.263 | 0.480 | 0.784 | 0.61 | 33 |
| GP 17 | <0.001 | <0.004 | <0.003 | 0.07 | 106 | 25 | 27.513 | 43.061 | 4.327 | 16.364 | 2.795 | 0.760 | 3.608 | 0.562 | 3.285 | 0.738 | 2.249 | 0.318 | 1.987 | 0.305 | 0.454 | 2.047 | 0.22 | 33 |
| GP 18 | <0.001 | <0.004 | <0.003 | 0.09 | 86 | 7 | 10.585 | 17.976 | 2.118 | 7.751 | 1.294 | 0.355 | 1.491 | 0.209 | 1.063 | 0.201 | 0.566 | 0.069 | 0.436 | 0.062 | 0.338 | 1.620 | 0.18 | 36 |
| GP 19 | <0.001 | <0.004 | <0.003 | 0.07 | 184 | 11 | 16.910 | 31.614 | 3.356 | 12.316 | 2.133 | 0.550 | 2.520 | 0.354 | 1.905 | 0.395 | 1.156 | 0.152 | 0.950 | 0.139 | 0.310 | 1.290 | 0.24 | 29 |
| GP 20 | <0.001 | <0.004 | <0.003 | 0.08 | 96 | 7 | 9.389 | 16.397 | 1.899 | 6.941 | 1.225 | 0.326 | 1.418 | 0.209 | 1.037 | 0.194 | 0.538 | 0.062 | 0.398 | 0.057 | 0.255 | 0.697 | 0.37 | 35 |
| GP 21 | <0.001 | <0.004 | <0.003 | 0.19 | 105 | 5 | 7.874 | 13.628 | 1.586 | 5.760 | 0.977 | 0.257 | 1.095 | 0.152 | 0.779 | 0.151 | 0.406 | 0.052 | 0.319 | 0.046 | 0.298 | 1.995 | 0.15 | 34 |
| GP 22 | <0.001 | <0.004 | <0.003 | 0.10 | 774 | 7 | 8.262 | 14.369 | 1.726 | 6.668 | 1.271 | 0.332 | 1.447 | 0.197 | 0.967 | 0.186 | 0.513 | 0.062 | 0.364 | 0.056 | 0.220 | 3.100 | 0.08 | 37 |
| GP 23 | <0.001 | <0.004 | <0.003 | 0.04 | 203 | 7 | 7.867 | 13.243 | 1.672 | 6.404 | 1.203 | 0.321 | 1.380 | 0.198 | 1.044 | 0.205 | 0.520 | 0.069 | 0.421 | 0.063 | 0.401 | 0.448 | 0.90 | 35 |
| GP 24 | <0.001 | <0.004 | <0.003 | 0.23 | 199 | 6 | 9.499 | 15.173 | 1.861 | 6.770 | 1.300 | 0.340 | 1.391 | 0.192 | 0.915 | 0.171 | 0.440 | 0.053 | 0.303 | 0.045 | 0.368 | 1.477 | 0.25 | 34 |
| GP 25 | <0.001 | <0.004 | 1 | 0.04 | 104 | 14 | 13.040 | 20.923 | 2.479 | 9.406 | 1.668 | 0.457 | 2.015 | 0.314 | 1.786 | 0.383 | 1.152 | 0.159 | 1.030 | 0.157 | 0.469 | 0.780 | 0.59 | 36 |
| GP 26 | <0.001 | <0.004 | <0.003 | 0.03 | 111 | 8 | 10.773 | 17.965 | 2.043 | 7.270 | 1.274 | 0.308 | 1.377 | 0.197 | 1.051 | 0.222 | 0.616 | 0.085 | 0.502 | 0.071 | 0.500 | 0.779 | 0.64 | 35 |
| GP 27 | <0.001 | <0.004 | <0.003 | 0.26 | 7914 | 42 | 65.134 | 104.063 | 13.581 | 50.121 | 8.572 | 2.185 | 9.303 | 1.248 | 5.953 | 1.161 | 3.135 | 0.369 | 2.119 | 0.302 | 1.016 | 2.998 | 0.34 | 36 |
| GP 28 | <0.001 | <0.004 | 0 | 0.41 | 3061 | 27 | 41.753 | 60.064 | 7.393 | 26.268 | 4.397 | 1.129 | 4.836 | 0.664 | 3.292 | 0.646 | 1.812 | 0.227 | 1.383 | 0.195 | 0.500 | 1.830 | 0.33 | 42 |
| GP 28rpt | | | | | | | | | | | | | | | | | | | | | | 1.470 | | |
| GP 29 | <0.001 | <0.004 | <0.003 | 0.05 | 76 | 7 | 15.102 | 21.185 | 2.180 | 7.393 | 1.102 | 0.280 | 1.390 | 0.188 | 1.023 | 0.225 | 0.695 | 0.096 | 0.608 | 0.088 | 0.228 | 0.460 | 0.60 | 30 |
| GP 30 | <0.001 | <0.004 | <0.003 | 0.03 | 98 | 5 | 10.816 | 16.722 | 1.940 | 6.754 | 1.077 | 0.268 | 1.188 | 0.155 | 0.746 | 0.149 | 0.417 | 0.049 | 0.317 | 0.044 | 0.231 | 0.240 | 1.45 | 34 |
| GP 31 | <0.001 | <0.004 | <0.003 | 0.04 | 80 | 5 | 13.053 | 19.796 | 2.380 | 8.145 | 1.262 | 0.316 | 1.380 | 0.169 | 0.805 | 0.158 | 0.423 | 0.052 | 0.307 | 0.044 | 0.224 | 0.167 | 1.34 | 33 |
| GP 32 | <0.001 | <0.004 | <0.003 | 0.03 | 88 | 8 | 25.425 | 34.275 | 4.239 | 14.539 | 2.137 | 0.599 | 2.420 | 0.296 | 1.297 | 0.251 | 0.645 | 0.074 | 0.436 | 0.061 | 0.219 | 0.191 | 1.15 | 33 |
| GP 33 | 1 | <0.004 | 5 | 1.91 | 4227 | 20 | 40.075 | 60.483 | 8.162 | 30.298 | 5.234 | 1.436 | 5.354 | 0.706 | 3.146 | 0.574 | 1.504 | 0.160 | 0.880 | 0.125 | 0.659 | 1.190 | 0.43 | 35 |
| GP 33A | <0.001 | <0.004 | <0.003 | 0.01 | 70 | 6 | 11.355 | 18.851 | 2.112 | 7.435 | 1.169 | 0.279 | 1.334 | 0.173 | 0.836 | 0.166 | 0.461 | 0.056 | 0.346 | 0.050 | 0.187 | 0.373 | 0.50 | 35 |
| GP 34 | <0.001 | <0.004 | <0.003 | 0.09 | 115 | 6 | 11.060 | 18.819 | 2.092 | 7.407 | 1.231 | 0.303 | 1.345 | 0.187 | 0.941 | 0.200 | 0.558 | 0.071 | 0.459 | 0.067 | 0.235 | 0.603 | 0.39 | 30 |
| GP 35 | <0.001 | <0.004 | <0.003 | 0.20 | 96 | 11 | 17.682 | 26.695 | 3.032 | 11.116 | 1.874 | 0.461 | 2.213 | 0.304 | 1.574 | 0.327 | 0.931 | 0.119 | 0.718 | 0.107 | 0.413 | 2.084 | 0.20 | 34 |
| GP 36 | <0.001 | <0.004 | <0.003 | 0.71 | 123 | 5 | 8.791 | 13.007 | 1.621 | 5.906 | 0.963 | 0.228 | 1.027 | 0.133 | 0.658 | 0.129 | 0.339 | 0.042 | 0.266 | 0.038 | 0.347 | 0.885 | 0.39 | 37 |
| GP 37 | <0.001 | <0.004 | <0.003 | 0.06 | 104 | 6 | 9.381 | 14.936 | 1.572 | 5.696 | 0.897 | 0.211 | 1.048 | 0.141 | 0.725 | 0.146 | 0.438 | 0.053 | 0.338 | 0.046 | 0.206 | 1.187 | 0.17 | 42 |
| GP 38 | <0.001 | <0.004 | <0.003 | 0.10 | 97 | 3 | 6.270 | 10.162 | 1.261 | 4.348 | 0.663 | 0.154 | 0.700 | 0.089 | 0.400 | 0.075 | 0.215 | 0.023 | 0.154 | 0.021 | 0.264 | 0.350 | 1.67 | 37 |
| GP 39 | <0.001 | <0.004 | <0.003 | 0.05 | 167 | 6 | 13.982 | 19.761 | 2.258 | 8.044 | 1.357 | 0.332 | 1.481 | 0.201 | 0.969 | 0.199 | 0.549 | 0.066 | 0.400 | 0.058 | 0.190 | 0.190 | 1.00 | 30 |
| GP 40 | <0.001 | <0.004 | <0.003 | 0.02 | 90 | 8 | 8.824 | 14.449 | 1.567 | 5.800 | 0.936 | 0.234 | 1.104 | 0.150 | 0.754 | 0.154 | 0.434 | 0.053 | 0.310 | 0.044 | 0.171 | 0.300 | 0.72 | 53 |
| GP 40 A | | | | | | | | | | | | | | | | | | | | | | | | |

**Appendix 1.** (*continued*)

| Sample id # | Co | Ni | Cu | Mo | P | Y | La | Ce | Pr | Nd | Sm | Eu | Gd | Tb | Dy | Ho | Er | Tm | Yb | Lu | Th | U | Th/U | Y/Ho |
|---|---|---|---|---|---|---|---|---|---|---|---|---|---|---|---|---|---|---|---|---|---|---|---|---|
| GP 41 | <0.001 | <0.004 | 4 | 0.17 | 125 | | | | | | | | | | | | | | | | | 0.908 | | |
| GP 41 A | <0.001 | <0.004 | 3 | 0.21 | 72 | | | | | | | | | | | | | | | | | 0.300 | | |
| GP 42 | <0.001 | <0.004 | 4 | 0.19 | 58 | | | | | | | | | | | | | | | | | 0.227 | | |
| GP 43 | <0.001 | <0.004 | 4 | 0.44 | 95 | | | | | | | | | | | | | | | | | 0.150 | | |
| GP 44 | <0.001 | <0.004 | 4 | 0.34 | 101 | | | | | | | | | | | | | | | | | 0.381 | | |
| GP 45 | <0.001 | <0.004 | 2 | 0.08 | 72 | | | | | | | | | | | | | | | | | 0.240 | | |
| GP 46 | <0.001 | <0.004 | 2 | 0.09 | 112 | | | | | | | | | | | | | | | | | 0.200 | | |
| GP 47 | <0.001 | <0.004 | 2 | 0.17 | 150 | | | | | | | | | | | | | | | | | 0.410 | | |
| GP 48 | <0.001 | <0.004 | 4 | 0.38 | 145 | | | | | | | | | | | | | | | | | 0.770 | | |
| GP 49 | <0.001 | <0.004 | 3 | 1.28 | 582 | | | | | | | | | | | | | | | | | 1.148 | | |
| GP 50 | <0.001 | <0.004 | 3 | 0.74 | 159 | | | | | | | | | | | | | | | | | 0.885 | | |
| GP 51 | <0.001 | <0.004 | 3 | 0.52 | 154 | | | | | | | | | | | | | | | | | 0.429 | | |
| GP 52 | <0.001 | <0.004 | 3 | 0.26 | 334 | | | | | | | | | | | | | | | | | 0.364 | | |
| GP 53 | <0.001 | <0.004 | <0.003 | 0.19 | 110 | | | | | | | | | | | | | | | | | 0.107 | | |
| GP 54 | <0.001 | <0.004 | <0.003 | 0.68 | 146 | | | | | | | | | | | | | | | | | 0.167 | | |
| GP 55 | <0.001 | <0.004 | <0.003 | 0.33 | 122 | | | | | | | | | | | | | | | | | 0.722 | | |
| GP 56 | <0.001 | <0.004 | <0.003 | 0.81 | 116 | | | | | | | | | | | | | | | | | 0.865 | | |
| GP 57 | <0.001 | <0.004 | <0.003 | 0.34 | 109 | | | | | | | | | | | | | | | | | 1.215 | | |
| GP 58 | <0.001 | <0.004 | <0.003 | 0.30 | 115 | | | | | | | | | | | | | | | | | 1.006 | | |
| GP 59 | <0.001 | <0.004 | <0.003 | 0.62 | 162 | | | | | | | | | | | | | | | | | 1.249 | | |
| GP 59rpt | | | | | | | | | | | | | | | | | | | | | | | | |
| GP 60 | <0.001 | <0.004 | <0.003 | 0.47 | 130 | | | | | | | | | | | | | | | | | 2.142 | | |
| GP 61 | | | | | | | | | | | | | | | | | | | | | | | | |
| GP 62 | | | | | | | | | | | | | | | | | | | | | | | | |
| GP 63 | | | | | | | | | | | | | | | | | | | | | | | | |
| GP 64 | | | | | | | | | | | | | | | | | | | | | | | | |
| GP 65 | | | | | | | | | | | | | | | | | | | | | | | | |
| GP 66 | | | | | | | | | | | | | | | | | | | | | | | | |
| GP 67 | | | | | | | | | | | | | | | | | | | | | | | | |
| GP 68 | | | | | | | | | | | | | | | | | | | | | | | | |
| GP 69 | | | | | | | | | | | | | | | | | | | | | | | | |
| GP 70 | | | | | | | | | | | | | | | | | | | | | | | | |
| GP 71 | | | | | | | | | | | | | | | | | | | | | | | | |
| GP 72 | | | | | | | | | | | | | | | | | | | | | | | | |
| GP 73 | | | | | | | | | | | | | | | | | | | | | | | | |
| GP 74 | | | | | | | | | | | | | | | | | | | | | | | | |
| GP 75 | | | | | | | | | | | | | | | | | | | | | | | | |
| GP 76 | | | | | | | | | | | | | | | | | | | | | | | | |
| GP 77 | | | | | | | | | | | | | | | | | | | | | | | | |
| GP 78 | | | | | | | | | | | | | | | | | | | | | | | | |
| GP 79 | | | | | | | | | | | | | | | | | | | | | | | | |
| GP 80 | | | | | | | | | | | | | | | | | | | | | | | | |
| GP 81 | | | | | | | | | | | | | | | | | | | | | | | | |
| GP 82 | | | | | | | | | | | | | | | | | | | | | | | | |